GenoMed Connect
ISSN: 3105-3645
2026, Article ID. 2026.0030, Cite as: https://doi.org/10.69709/GenomC.2026.133666

SCIFINITI PUBLISHING

Review Article

OPEN ACCESS

Metabolic Reprogramming in Brain Metastases: Integrating Spatial Omics with Non-Spatial Mechanistic Evidence

Hongbin Lan[✉,1,*], **Xiuqi Wang**[✉,1], **Zhen Zeng**[✉,2]

[1] Division of Applied Oral Sciences & Community Dental Care, Faculty of Dentistry, The University of Hong Kong, Hong Kong SAR, China
[2] Department of Thoracic Surgery and Institute of Thoracic Oncology, West China Hospital, Sichuan University, Chengdu 610041, China

Article History
Received: May 03, 2026 Accepted: September 30, 2026 Published: October 26, 2026

Abstract
Brain metastases (BrMs) arise within a metabolically specialized environment in which nutrient availability and interactions with neural, vascular, and immune cells can influence tumor growth. Bulk and single-cell studies have identified metabolic alterations, whereas spatial approaches add information on their regional and cellular context. This review examines spatial transcriptomics, proteomics, and mass spectrometry imaging alongside biochemical measurements and functional studies, with a focus on central carbon metabolism, glutamate-glutamine metabolism, lipid handling, and oxidative phosphorylation. The available spatial studies describe regional differences in metabolism-associated molecular programs, lipid abundance, and isotope labeling. Complementary experiments implicate tumor-cell synthesis, host-derived substrate supply, and mitochondrial activity as contributors to growth in BrM models. These findings suggest that similar metabolic functions recur across tumor origins, although it remains uncertain whether these functions depend on the same molecular pathways. Some BrM-associated features are also detectable in primary tumors, which suggests that these states may precede brain colonization. The review therefore discusses how matched-site comparisons, tracing, and cell-specific perturbation could help distinguish pre-existing features from local adaptations and clarify the sources and requirements of key metabolites. Linking tissue findings to longitudinal imaging and liquid-biopsy measurements could support the evaluation of candidate targets and biomarkers and help overcome the limited opportunities for repeated tissue sampling.

Keywords:
brain metastases; spatial multi-omics; metabolic reprogramming; tumor microenvironment heterogeneity; metabolic-immune crosstalk; metabolic vulnerabilities; metabolic niches

1. Introduction

Brain metastases (BrMs) are a frequent complication of advanced solid tumors, particularly lung cancer, breast cancer, and melanoma, and they pose a major clinical challenge [1]. Despite advances in surgery, radiotherapy, targeted therapy, and immunotherapy, patient outcomes remain poor [2]. Disseminated tumor cells adapt to a specialized brain microenvironment shaped by the blood-brain barrier (BBB), restricted nutrient availability, and distinct neurovascular and neuroimmune interactions [2]. Colonization therefore requires metabolic adaptation that sustains energy production, redox balance, and biosynthesis under conditions that differ from those at the primary site [3]. These adaptations remain incompletely understood because conventional molecular approaches cannot fully resolve the spatial and functional organization of the metastatic niche.

Bulk and single-cell omics have substantially advanced the understanding of cancer progression and metastatic adaptation, but each provides only a partial view of BrM biology. Bulk analyses average signals across heterogeneous cell populations and anatomical re-

* **Corresponding Author:**
Hongbin Lan, Division of Applied Oral Sciences & Community Dental Care, Faculty of Dentistry, The University of Hong Kong, Hong Kong SAR, China, hongbinl@connect.hku.hk

© 2026 Copyright by the Authors.
Licensed as an open access article using a CC BY 4.0 license.

gions, which obscures localized metabolic programs and phenotypic gradients within the tumor microenvironment (TME) [4]. Single-cell and single-nucleus ribonucleic acid (RNA) sequencing improve cellular resolution, but the tissue dissociation required by these approaches disrupts the spatial relationships needed to interpret cell-cell and cell-niche interactions [5]. This limitation is particularly relevant to metabolism, which is strongly shaped by local oxygen tension, nutrient access, vascular proximity, and stromal crosstalk [6]. Understanding metabolic adaptation in BrMs therefore requires approaches that preserve tissue architecture while capturing molecular heterogeneity.

Spatially resolved technologies enable BrMs to be studied as anatomically organized ecosystems rather than uniform lesions. By preserving tissue context, they can localize metabolic programs relative to vascular or glial niches and determine whether those programs coincide with hypoxic stress, immune suppression, or therapeutic vulnerability [7,8]. Emerging studies implicate interactions with astrocytes, microglia, macrophages, endothelial cells, and other stromal elements [9,10] and report regional heterogeneity that is associated with the vascular, immune, and glial context [11–13]. Most studies, however, infer metabolism from RNA or protein, include only modest cohorts, and lack direct measurements of metabolite abundance or flux. Further integration with direct metabolic measurements and functional perturbation would therefore help clarify pathway activity and assess potential therapeutic vulnerabilities.

This review summarizes current knowledge of metabolic reprogramming in BrMs and examines how spatially resolved approaches refine its interpretation. The review first outlines the spatial technologies used to interrogate the BrM microenvironment and then assesses evidence for central carbon metabolism, glutamate-glutamine utilization, lipid remodeling, and oxidative phosphorylation (OXPHOS). The review concludes by considering translational implications, current limitations, and priorities for spatially informed metabolic research in BrMs.

1.1. Literature Search and Study Selection

A focused narrative search of PubMed and Google Scholar was conducted, combining brain metastasis terms with spatial transcriptomics, spatial proteomics, mass spectrometry imaging, spatial metabolomics, and metabolic terms including glycolysis, glutamine, lipid metabolism, oxidative phosphorylation, and isotope tracing. The reference lists and citing articles of key reports were also screened. Priority was given to human BrM spatial studies, matched-site comparisons, and direct metabolic measurements, followed by BrM-specific functional studies. Evidence from other tumors was included for methodological or translational context and is explicitly identified as indirect evidence. Targeted reference and ClinicalTrials.gov checks were updated through 13 September 2026. This narrative review was not registered with a protocol and makes no claim to systematic or exhaustive coverage.

2. The Spatial Toolkit: Decoding the Metabolic Microenvironment In Situ

A growing range of spatial technologies is used to characterize metabolism-associated features in BrMs while preserving tissue architecture. These platforms differ in molecular coverage, spatial resolution, and the metabolic inferences that they support, thereby providing complementary views of the BrM microenvironment.

Spatial transcriptomics, including array-based platforms such as 10x Visium and imaging-based approaches such as multiplexed error-robust fluorescence in situ hybridization (MERFISH) and Xenium, maps gene-expression programs across tissue sections [14–16]. For example, in a melanoma BrM study, spatial profiling (Slide-seqV2) identified opposing glycolysis- and OXPHOS-associated RNA programs within a single lesion, illustrating metabolic heterogeneity at the level of gene expression [12]. These maps localize candidate metabolic programs; however, post-transcriptional and post-translational regulation limits the inference of enzyme activity from RNA abundance [17].

Multiplexed spatial proteomic technologies quantify proteins in defined tissue regions or cells. Examples include imaging mass cytometry (IMC) [5], CO-Detection by indEXing (CODEX), and digital spatial profiling (DSP). Mapping metabolic enzymes and signaling mediators alongside cell-type markers links candidate pathways to tumor, glial, vascular, and immune compartments. However, protein abundance does not necessarily reflect enzyme activity or metabolic flux. Integrating these maps with direct metabolic measurements would help clarify the functional significance of the observed spatial patterns.

Mass spectrometry imaging (MSI), particularly matrix-assisted laser desorption/ionization mass spectrometry imaging (MALDI-MSI), measures metabolite- and lipid-associated ion signals at defined locations across tissue sections, thereby revealing spatial distributions that complement RNA and protein expression profiles [18,19]. However, regional differences in signal intensity can reflect both metabolite abundance and local ionization ef-

2026, Vol. 3, Article ID. 2026.0030
https://doi.org/10.69709/GenomC.2026.133666

fects, complicating quantitative comparisons [20]. A recent workflow using isotope-labeled internal standards improved pixel-wise normalization and relative quantification in brain and kidney tissue, illustrating how such effects can be reduced to support more reliable regional comparisons [21]. Whereas isotope-labeled internal standards improve abundance measurements, administering labeled nutrients before tissue collection enables MSI to trace their metabolic fate across tissue regions [22]. Samarah et al. combined stable-isotope tracing with MSI in mouse liver and intestine to visualize the incorporation of labeled nutrients into downstream metabolites and identify regional differences in substrate utilization [22]. Initial isotope-imaging studies have already examined substrate labeling in BrM tissue, as discussed in Section 4.1. Extending these measurements across patients could clarify regional differences in substrate use.

Combining different spatial measurements enables gene and protein expression to be examined alongside metabolite distributions within a common tissue context. Computational frameworks can align spatial transcriptomic, proteomic, and MSI data across adjacent or co-registered tissue sections [23–25], while same-section workflows reduce uncertainty arising from anatomical differences between adjacent sections [23,24,26,27]. Recent optical platforms further extend this integration to cell-resolved chemical measurements. For example, Raman Enhanced Delineation of Cell Atlases in Tissues (REDCAT) combines Raman-based chemical imaging, optical redox readouts, and multiplexed immunofluorescence on the same section to link lipid and redox-related features to specific cell types [28]. Applying REDCAT in human lymphoid and liver tissues demonstrates how this approach can characterize metabolic heterogeneity within defined cellular populations [28]. Adapting such workflows to BrMs could help distinguish tumor cell metabolic features from those of neighboring glial, vascular, and immune cells.

Together, spatial RNA, protein, and chemical measurements link lesion-level metabolic observations to local cellular neighborhoods. Integration with appropriately designed tracing and functional perturbation would help establish which localized programs are active and would allow their potential as therapeutic vulnerabilities to be assessed.

3. Spatial Organization in BrMs

In BrMs, tumor cells interact with vascular, glial, and immune cells within spatially heterogeneous local environments [9]. Brain-specific vascular structures, including the neurovascular unit and the BBB or blood-tumor barrier (BTB), regulate access to the tissue, whereas astrocytes, microglia, and neurons contribute specialized metabolic functions [2]. This spatial arrangement creates cellular neighborhoods in which tumor-host interactions may influence colonization and treatment response [5]. This section focuses on the microanatomical organization within and around parenchymal BrMs, considering perivascular regions, the lesion interior, and the brain-tumor interface with adjacent brain tissue before turning to finer-scale neuronal contacts.

The perivascular region is one major niche, where metastatic cells interact with endothelial cells, pericytes, and astrocytic endfeet [29]. Endothelial barrier properties, supported and regulated by pericytes and astrocytes, help control exchange between the circulation and the surrounding tissue [29]. In BrMs, BTB permeability varies within and between lesions, as shown by permeability measurements and heterogeneous drug accumulation in mouse models of breast-cancer BrM [30]. These observations raise a related metabolic question, namely whether this vascular heterogeneity is accompanied by differences in local nutrient availability and in substrate utilization by tumor and neighboring cells.

Lipid accumulation also differs between perivascular and perinecrotic regions. For example, fluorescence imaging of human central nervous system (CNS) metastases originating from kidney cancer, melanoma, and lung cancer revealed lipid-droplet-rich, carbonic anhydrase IX (CA-IX)-positive perinecrotic regions, in contrast to lipid-droplet-poor perivascular regions [31]. This regional contrast illustrates how tissue architecture can coincide with differences in lipid storage within metastatic tissue.

The brain-tumor interface, at the boundary with adjacent brain tissue, ranges from a well-demarcated border to an infiltrative margin. Histopathological analysis of human BrM autopsy specimens identified well-demarcated borders, perivascular extensions of tumor-cell clusters, and diffuse infiltration of individual tumor cells into the surrounding brain tissue [32]. Along these margins, metastatic cells come into contact with reactive astrocytes, microglia, and neurons [10,33,34]. This contrast between circumscribed and infiltrative growth also extends to immune organization. For example, spatial profiling of human BrMs revealed a lymphocyte-rich band separating the tumor from the surrounding brain in minimally invasive lesions, whereas this organization was largely absent from highly invasive lesions [35]. Thus, the interface differs across lesions in both the extent of tumor infiltration and the arrangement of neighboring host cells.

At a finer spatial scale, tumor cells can establish close contacts with neuronal structures. In breast-cancer

2026, Vol. 3, Article ID. 2026.0030
https://doi.org/10.69709/GenomC.2026.133666

BrM mouse models, tumor-cell protrusions were observed next to excitatory synapses in pseudo-tripartite arrangements [36]. These observations extend the description of BrM organization from tissue compartments and cellular neighborhoods to subcellular contacts.

Together, the spatial complexity of BrMs and their interfaces with surrounding brain tissue suggests that metabolic states and tumor-host interactions differ across local environments. This organization complicates the interpretation of lesion-level metabolic profiles but also justifies spatially resolved studies that relate metabolic features to specific tissue regions and cellular neighborhoods. Against this spatial background, the following section examines metabolic adaptations in BrMs and considers how their interpretation depends on local context.

4. Metabolic Reprogramming in BrMs: Single-Cell and Spatial Insights

Studies of metabolic reprogramming in BrMs implicate central carbon metabolism, glutamate-glutamine metabolism, lipid remodeling, and OXPHOS in tumor growth and tumor-host interactions. Direct spatial measurements of these processes remain limited; current understanding therefore relies largely on bulk and single-cell profiling, metabolic tracing, and functional studies. This section discusses these findings alongside spatial observations, examining the cellular and anatomical context of metabolic programs and their similarities and differences across primary-tumour origins. Figure 1 summarizes the major metabolic programs and their reported spatial context in BrMs.

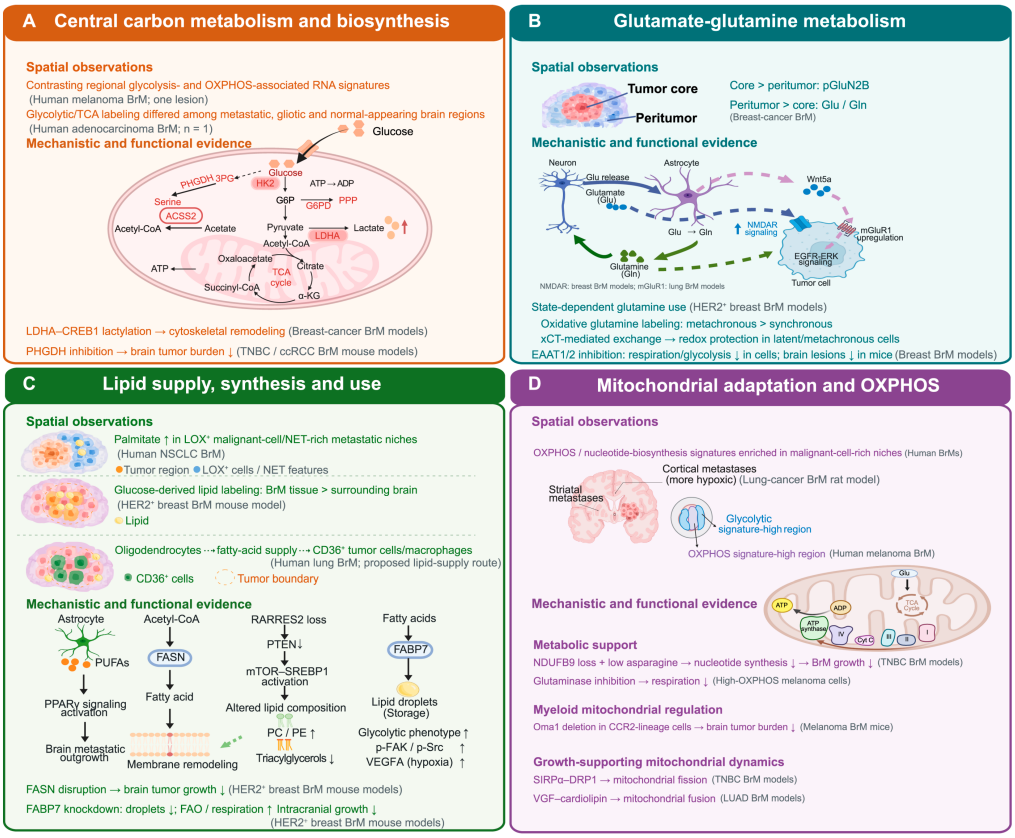

Figure 1: Spatial observations and complementary mechanisms of metabolic reprogramming in BrMs. Each panel separates regional observations from mechanistic and functional findings obtained in the indicated tumor origins and experimental settings. (**A**) Central carbon metabolism and biosynthesis, linking regional glycolytic and TCA-associated measurements to pathways supporting carbon utilization and growth. (**B**) Glutamate-glutamine metabolism, distinguishing regional metabolite and receptor-phosphorylation patterns from neuronal and glial signaling, substrate transport, and state-dependent glutamine use. (**C**) Lipid supply, synthesis, and use, relating regional lipid enrichment and isotope labeling to tumor-cell synthesis, candidate glial supply, membrane composition, and lipid storage. (**D**) Mitochondrial adaptation and OXPHOS, combining regional transcriptional and oxygenation differences with experimental findings on biosynthetic support, myeloid regulation, and mitochondrial dynamics. Findings from different studies are juxtaposed for comparison rather than combined into a single validated pathway. Arrows indicate the relationships or directions reported in the specified settings; dotted donor-recipient links denote a proposed supply route. Metabolite abundance, transcript enrichment, and isotope labeling are distinct readouts and do not, by themselves, establish quantitative flux or a shared therapeutic dependency.

2026, Vol. 3, Article ID. 2026.0030
https://doi.org/10.69709/GenomC.2026.133666

4.1. Central Carbon Metabolism and Associated Biosynthetic Pathways

Central carbon metabolism links glucose breakdown and tricarboxylic acid (TCA) cycle oxidation to pathways that supply biosynthetic precursors. BrM studies implicate glycolysis, acetate utilization, and linked biosynthetic pathways, but it remains unclear whether glycolytic or TCA-cycle activity is consistently increased across primary-tumor origins [9]. Spatial profiling and isotope imaging provide complementary information on regional metabolic programs and substrate use, whereas functional studies examine how these processes support BrM growth.

Spatial transcriptomics provides a starting point for examining how central carbon metabolism varies within lesions. In the treatment-naive melanoma cohort of Biermann et al., Slide-seqV2 profiled 16 sections, including 11 from BrMs and five from extracranial metastases. In one malignant-cell-rich BrM, glycolysis- and OXPHOS-associated transcriptional signatures showed contrasting regional distributions [12]. In addition to regional variation within BrMs, spatial profiling can reveal metabolic programs that are shared with the primary tumor. In three patients with triple-negative breast cancer (TNBC), Visium profiling of matched residual primary tumors and BrMs identified a glycolysis-related gene module common to both sites [37]. Thus, a metabolic program detected in BrMs may have been retained from the primary tumor rather than acquired in the brain. Together, these studies describe regional variation within BrMs and metabolic gene-expression programs shared with primary tumors, whereas direct metabolic measurements are needed to clarify local pathway activity.

Isotope imaging adds a spatial readout of glucose-derived carbon incorporation to the transcriptional patterns described above. In a study of two patients with glioblastoma and one patient with an adenocarcinoma BrM, intraoperative [U-^{13}C]glucose infusion was followed by desorption electrospray ionization mass spectrometry imaging (DESI-MSI) of resected tissue. Analysis of seven regions from the BrM, at a pixel size of 65 μm, identified differences in labeled glycolytic and TCA-associated metabolites among metastatic tissue, gliotic tissue, and normal-appearing brain [38]. This single-patient observation provides an initial view of regional glucose metabolism in human BrM, whereas the quantitative relationship between these labeling patterns and local pathway flux remains unclear.

The spatial observations described above reveal regional metabolic differences but do not establish which enzymes contribute to tumor growth. Cell and animal experiments address this question by perturbing glycolytic enzymes and their regulators in BrM models. Hexokinase 2 (HK2) catalyzes glucose phosphorylation at the entry point of glycolysis. In 123 surgically resected human breast-cancer BrMs, high HK2 immunoreactivity was associated with shorter post-craniotomy survival, whereas HK2 knockdown reduced proliferation of 231-BR cells under glucose-limiting conditions [39]. Another glycolytic enzyme, phosphoglycerate mutase 1 (PGAM1), has been implicated in non-small cell lung cancer (NSCLC) BrM growth through its stabilization by SEC61 translocon subunit gamma (SEC61G), an endoplasmic-reticulum translocon component [40]. Experiments in brain-selected lung-cancer sublines and intracardiac mouse models linked SEC61G-mediated PGAM1 stabilization to increased glycolysis and brain metastatic growth. Single-cell profiling and patient-tissue immunohistochemistry provided complementary data on SEC61G expression [40]. These findings suggest that glycolytic enzymes and their regulators can support growth in the breast- and lung-cancer BrM models examined, whereas their contribution within the spatially mapped regions remains to be tested.

Studies of lactate production and protein lactylation further link glycolysis to tumor-cell behavior and immune regulation. Lactate dehydrogenase A (LDHA) converts pyruvate, the end product of glycolysis, to lactate. In breast cancer, LDHA staining in primary TNBC specimens and serum lactate dehydrogenase (LDH) levels were associated with subsequent brain relapse [41]. Mechanistic studies in breast-cancer models linked LDHA-mediated cyclic adenosine monophosphate response element-binding protein 1 (CREB1) lactylation to cytoskeletal remodeling, whereas LDHA knockdown reduced brain tumor burden in mice [42]. Lung-cancer studies examined myeloid-cell responses. An intracranial Lewis lung carcinoma (LLC) model showed lactate accumulation, and murine macrophage experiments linked Rac family small GTPase 2 (RAC2) lactylation to altered polarization. Human observations were limited to histone H3 lysine 18 lactylation (H3K18la) staining in two primary-BrM pairs and two non-BrM primary tumors [43]. These findings motivate spatial studies to determine whether lactate-rich regions coincide with tumor-cell lactylation or distinct macrophage states, and whether these relationships vary by primary tumor origin.

Glucose metabolism also feeds the pentose phosphate pathway (PPP), which supplies reduced nicotinamide adenine dinucleotide phosphate (NADPH) and nucleotide precursors [44]. In a tissue-microarray study of 126 breast-cancer metastases, including 36 brain lesions, positivity for the pathway enzyme glucose-6-phosphate dehydrogenase (G6PD) was most frequent in BrMs, al-

though the molecular subtype composition differed across metastatic sites [44].

Beyond glucose, acetate can fuel TCA-cycle metabolism in human BrMs. Proteomic comparisons of breast-cancer brain- and bone-metastatic variants identified differences in central carbon enzymes [45]. Intraoperative [1,2-^{13}C]acetate infusion in four brain-tumor patients, including one breast-cancer BrM and one NSCLC BrM, produced labeling, detected by nuclear magnetic resonance (NMR), consistent with acetate oxidation [46]. The regional distribution of this substrate use within BrMs remains unclear.

Acetyl-CoA synthetase 2 (ACSS2) generates acetyl-coenzyme A (acetyl-CoA) from acetate, linking alternative carbon use to biosynthesis. Brain-penetrant ACSS2 inhibitors reduced breast cancer BrM growth in cell-based, brain-slice, and mouse models [47]. Further perturbation studies linked ACSS2 to ferroptosis suppression and reduced brain metastatic growth after inhibition; human observations comprised phosphorylated ACSS2 staining in 43 BrMs of mixed origin [48]. These preclinical findings support spatial investigation of acetate-related vulnerabilities, although the requirement for ACSS2 in acetate oxidation in patient BrMs remains unclear.

Phosphoglycerate dehydrogenase (PHGDH) catalyzes the first step of serine biosynthesis from the glycolytic intermediate 3-phosphoglycerate. Transcript profiling of patient tissue showed serine-pathway enrichment in melanoma BrMs versus matched extracranial metastases, whereas immunohistochemistry detected high PHGDH expression in 27 of 30 breast-cancer BrMs [49]. Glucose tracing and PHGDH inhibition in BrM-derived or brain-selected systems linked serine synthesis to growth under serine/glycine limitation. PH-755 reduced intracranial tumor burden after tumors had formed in TNBC and clear-cell renal cell carcinoma (ccRCC) models; inhibitor testing in melanoma was limited to cell culture [49]. It remains unclear whether spatial differences in nutrient availability influence this sensitivity within patient BrMs.

Branched-chain amino-acid aminotransferase 1 (BCAT1) uses the TCA intermediate α-ketoglutarate (α-KG) for branched-chain amino-acid transamination. BCAT1 staining was higher in NSCLC BrMs than in largely unpaired primary lung adenocarcinoma (LUAD) specimens [50]. A549/H1299 cell and intracranial H1299 xenograft experiments linked BCAT1-dependent α-KG depletion to altered AlkB homolog 5 (ALKBH5) activity and N^6-methyladenosine (m^{6}A) regulation [50]. In contrast to the biosynthetic role of serine synthesis, this mechanism links central carbon metabolism to RNA regulation.

Glucose-sensitive and pyruvate-based imaging provide additional spatial information on central carbon metabolism at the scale of lesions and brain regions. Dynamic glucose-enhanced chemical exchange saturation transfer (DGE-CEST) signals were elevated relative to contralateral brain in two of four BrMs, although blood–brain barrier leakage complicates their interpretation as a measure of glucose uptake [51]. In 18 patients with 44 BrMs, pretreatment hyperpolarized [1-^{13}C]pyruvate magnetic resonance imaging (MRI) detected a higher lactate-to-bicarbonate signal ratio in lesions that subsequently progressed after stereotactic radiosurgery [52]. The association links a regional metabolic readout to treatment outcome, but the cohort was small, and the spatial resolution was 1.5 cm. By contrast, a separate study of 12 patients and 46 controls found higher lactate-to-pyruvate and bicarbonate-to-pyruvate ratios in normal-appearing brain, after excluding tumor-containing regions and regions that were abnormal on T2-weighted fluid-attenuated inversion recovery (T2-FLAIR) images [53]. Thus, these studies provide spatially localized observations in different compartments, and lesion metabolism should be distinguished from changes in surrounding or remote brain when interpreting regional metabolic variation.

Central carbon metabolism in BrMs encompasses glucose oxidation, lactate-related regulation, acetate use, and biosynthetic pathways. Spatial transcriptomics and isotope imaging reveal regional gene-expression and isotope-labeling patterns, whereas genetic and pharmacological perturbations identify candidate functional requirements in specific cancer models. It remains unclear whether these requirements are shared across primary-tumor origins. Integrating spatial information with functional testing could clarify whether regions with distinct substrate use depend on the same enzymes or harbor different metabolic vulnerabilities.

4.2. Glutamate-Glutamine Metabolism

Glutamate-related adaptations in BrMs involve both receptor signaling and substrate use. In breast-cancer BrM models, microscopy localized tumor-cell protrusions beside neuronal synapses, whereas neuronal cocultures and GRIN2B (glutamate ionotropic receptor NMDA type subunit 2B) perturbation in intracardiac mouse models linked glutamate-responsive N-methyl-D-aspartate receptor (NMDAR) signaling to metastatic growth [36]. Paired human primary-tumor and BrM specimens provided complementary evidence of phosphorylated GluN2B (pGluN2B), the NMDAR subunit encoded by GRIN2B [36]. These anatomical observations raise the

2026, Vol. 3, Article ID. 2026.0030
https://doi.org/10.69709/GenomC.2026.133666

question of whether glutamate availability and receptor activation peak in the same regions.

Regional measurements in breast-cancer BrMs suggest that receptor phosphorylation and metabolite abundance need not peak in the same compartment. Biochemical analysis of manually delineated human tissue regions found higher glutamate, glutamine, and their combined pool (Glx) in peritumoral tissue, whereas immunohistochemistry localized stronger pGluN2B staining to the tumor core [54]. This regional contrast suggests that tissue metabolite abundance alone may not predict receptor signaling intensity. At the lesion scale, glutamine positron emission tomography (PET) in the same study detected higher tracer uptake in brain lesions than in paired mammary tumors in six mice, whereas clinical imaging was limited to one woman with a breast-cancer BrM [54]. These tissue and imaging measurements provide regional context, although metabolite abundance and tracer uptake do not directly measure cell-specific metabolic flux.

Functional studies help explain how glial signals can alter tumor-cell responses to local glutamate. In human lung cancer cells co-cultured with mouse-derived mixed glia, and in corresponding mouse BrM models, astrocyte-derived Wnt5a induced metabotropic glutamate receptor 1 (mGluR1) through prickle planar cell polarity protein 1 (PRICKLE1) and RE1-silencing transcription factor (REST), enabling glutamate-dependent epidermal growth factor receptor (EGFR) stabilization and extracellular signal-regulated kinase (ERK) activation [55]. Glial regulation of receptor signaling may therefore influence tumor-cell responses to local glutamate, alongside mechanisms controlling substrate supply and uptake, as discussed below.

Changes in host-cell metabolite handling and tumor-cell transport could contribute to regional differences in substrate availability. In breast-cancer systems, cell-culture, mouse brain-slice, and brain-interstitial analyses linked extracellular-vesicle-associated microRNA-199b-5p (miR-199b-5p) to the suppression of neuronal and astrocytic transporters and to greater extracellular availability of glutamate, glutamine, and lactate. Circulating miR-199b-5p was also associated with BrMs in 42 women with stage IV breast cancer [56]. Complementary experiments in brain-tropic breast-cancer cells linked nuclear factor κB (NF-κB) signaling to increased glutamate uptake mediated by excitatory amino-acid transporters 1 and 2 (EAAT1/EAAT2). Transporter inhibition reduced respiration and glycolytic readouts in culture, and it reduced brain-lesion formation in mice [57]. Together, these experiments suggest that altered substrate handling by host cells and increased uptake by tumor cells could both facilitate access to extracellular metabolites. It remains to be tested whether these mechanisms account for the spatial distributions observed in human BrMs.

Once substrates are available to tumor cells, their metabolic use may also depend on tumor-cell state. In human epidermal growth factor receptor 2 (HER2)-positive breast cancer models derived from HCC1954 and SKBR3 cells, phenotypic selection generated synchronous, latent, and metachronous states. In vivo [U-$^{13}C_5$]glutamine tracing showed greater oxidative labeling in metachronous than synchronous lesions, whereas comparisons involving latent cells were performed in vitro. Latent and metachronous cells also relied on cystine-glutamate exchange mediated by the xCT antiporter for redox control, indicating that glutamate handling contributes to antioxidant protection in addition to glutamine oxidation [58]. Immunohistochemistry was used to assess xCT expression in seven matched HER2-positive primary and metachronous metastatic cases, although its contribution to redox control in patient lesions remains unclear [58]. Together, these findings suggest that glutamine use and glutamate-linked redox regulation may vary with tumor-cell state; how these experimentally selected states relate to clinical latency or spatial niches warrants further investigation.

Glutamate metabolism is also linked to γ-aminobutyric acid (GABA) production through glutamate decarboxylase 1 (GAD1). Comparative transcriptomic analysis found enrichment of a GABA-related gene set in brain tumors across models of four primary-tumor origins, suggesting a shared transcriptional response to the brain environment. Functional experiments in breast-cancer and melanoma models linked glia-induced GAD1 expression to glutamine utilization and redox regulation; GAD1 knockdown reduced brain metastases in mice [59]. The overlap across models supports investigating a recurring GABA-related adaptation, although the transcriptional finding is broader than the functional testing.

Within this GABA-related response, GABA accumulation and metabolic utilization may support tumor growth through distinct mechanisms. In NSCLC brain-tropic cells and mouse models, reduced forkhead box A2 (FOXA2) and 4-aminobutyrate aminotransferase (ABAT) expression was linked to GABA accumulation, NF-κB signaling, and astrocyte activation; patient analyses also found higher circulating GABA in patients with BrMs [60]. A smoking-linked lung-cancer study instead linked nicotine-induced microglial microRNA-32-3p (miR-32-3p) signaling to neuronal GABA release and tumor-cell GABA-shunt use in ex vivo and in vivo models. Analysis of patient tissue associated smoking history with perineural invasion, providing anatomical context, and, in mice, GABA-uptake inhibitors reduced brain-metastatic

progression [61]. These findings distinguish GABA accumulation from substrate use rather than implying uniformly increased GABA catabolism. The local balance between these processes and its therapeutic relevance in patient BrMs remain open questions.

Together, these studies link glutamate-glutamine metabolism to neural signaling, extracellular substrate handling, and state-dependent metabolic requirements. GABA-related findings recur across several cancer origins, but their functional importance may differ according to tumor state and microenvironment. Spatial microscopy, regional biochemistry, and imaging offer complementary information on cellular contacts and metabolite distribution. Integrating these observations with local measurements of substrate use and with perturbation experiments could clarify where receptor signaling, oxidative metabolism, and redox protection contribute to BrM growth.

4.3. Lipid Metabolism and Membrane Remodeling

Although the brain is lipid-rich, the availability of these lipids to metastatic cells may vary among local environments [62]. Cancer cells can acquire fatty acids through de novo synthesis or uptake and subsequently incorporate them into membrane lipids or store them in lipid droplets [63,64]. The relative importance of these routes may depend on both local lipid supply and tumor-cell regulation. This distinction matters when interpreting spatial lipid maps because enrichment within a lesion may reflect differences in lipid production, uptake, or subsequent use. Spatial measurements can locate lipid enrichment and isotope labeling, whereas complementary functional studies help assess which aspects of lipid metabolism support growth.

In HER2-amplified breast-cancer BrM models, spatial isotope imaging and functional experiments suggest that tumor growth in the brain is particularly sensitive to the disruption of fatty-acid synthesis. Fatty acid synthase (FASN) uses acetyl-CoA and malonyl-CoA, together with NADPH, to produce palmitate, a 16-carbon saturated fatty acid [63]. Tracing of glucose-derived carbon into this product revealed greater palmitate labeling in brain tumors than in mammary-fat-pad tumors. MALDI-MSI added regional context by localizing greater labeling of palmitate and other lipids to BT474 brain tumors than to surrounding brain tissue [63]. The labeling supports incorporation of glucose-derived carbon into tumor lipids, although its interpretation as an absolute synthesis rate would require further kinetic measurements. To test whether this synthetic activity supported growth, FASN was disrupted using clustered regularly interspaced short palindromic repeats (CRISPR) and CRISPR-associated protein 9 (Cas9). This disruption reduced tumor growth in the brain, with little effect in the mammary fat pad or liver, and pharmacological FASN inhibition also reduced intracranial growth, which suggests a site-dependent contribution of fatty-acid synthesis in these models [63]. Mechanistic experiments in NSCLC cells provide a possible explanation for how tumor cells sustain FASN expression. Insulin-like growth factor 2 messenger RNA-binding protein 3 (IGF2BP3) stabilized FASN messenger RNA (mRNA) and supported lipid accumulation, and intracranial implantation experiments linked this regulatory axis to brain tumor growth [65]. These findings suggest that sustained FASN expression may support lipid-dependent growth in the brain beyond HER2-amplified breast-cancer models, although the NSCLC experiments did not spatially resolve this mechanism [65].

Retinoic acid receptor responder 2 (RARRES2) has also been linked to lipid regulation in breast-cancer cells and to reduced tumor growth in experimental BrMs. In mouse models using 4T1 breast-cancer cells, RARRES2 overexpression reduced tumor growth following intracranial implantation and brain metastatic burden after intracardiac injection [66]. Mechanistic experiments in MDA-MB-231 cells linked RARRES2 overexpression to increased phosphatase and tensin homolog (PTEN) and reduced signaling through mechanistic target of rapamycin (mTOR) and sterol regulatory element-binding protein 1 (SREBP1) [66]. SREBP1 is a transcription factor that regulates lipogenic enzyme expression, thereby connecting this signaling pathway to lipid synthesis. Conversely, RARRES2 knockdown increased phosphatidylcholine and phosphatidylethanolamine, major membrane phospholipids, but reduced triacylglycerols used for lipid storage [66]. Together, these cell experiments suggest that RARRES2 influences both lipogenic signaling and lipid composition, but it remains unresolved whether these changes mediate its effects on BrM growth.

Spatial lipid measurements also reveal regional differences in lipid accumulation that may have several metabolic explanations. In a spontaneous breast-cancer BrM mouse model, MALDI-MSI localized long-chain acylcarnitines and selected phospholipids to a macrometastatic lesion [67]. Although acylcarnitines are involved in fatty-acid handling, their accumulation does not necessarily indicate increased oxidation. The study instead proposed an association with ischemia or hypoxia [67]. A different spatial pattern emerged from integrated spatial transcriptomics and airflow-assisted desorption electrospray ionization mass spectrometry imaging (AFADESI-MSI) of human primary NSCLC and

2026, Vol. 3, Article ID. 2026.0030
https://doi.org/10.69709/GenomC.2026.133666

BrM tissue, which linked palmitate-rich regions to lysyl oxidase (LOX)-positive malignant cells, neutrophil-rich niches, and programs related to neutrophil extracellular traps (NETs) and epithelial-mesenchymal transition (EMT) [68]. Palmitate exposure promoted EMT-associated changes in NSCLC cells, which provides a possible functional explanation for the spatial association [68]. However, these cell experiments did not establish the source of palmitate or its contribution to EMT within the human tissue regions. Lipid storage and oxidation provide another distinction to consider when interpreting such maps. In HER2-positive breast-cancer BrM models, knockdown of the intracellular fatty-acid-binding protein 7 (FABP7) reduced glycolytic readouts and lipid-droplet accumulation but increased fatty-acid oxidation (FAO) and mitochondrial respiration in cell assays. In these cells, FABP7 knockdown also reduced phosphorylation of focal adhesion kinase (FAK) and Src and attenuated hypoxia-induced accumulation of hypoxia-inducible factor 1α (HIF-1α) and expression of vascular endothelial growth factor A (VEGFA) mRNA. The same intervention also limited intracranial growth [64], which suggests that greater oxidative activity need not accompany greater tumor growth. These findings highlight why regional lipid enrichment should be interpreted alongside measurements of lipid use rather than as evidence of a particular metabolic dependency.

Relating tumor regions to neighboring cells can help identify potential sources of the fatty acids BrM cells use. In lung-cancer BrMs, human single-cell and spatial transcriptomics, together with lipidomics and functional experiments, implicated oligodendrocytes as a potential source [69]. Spatial data placed oligodendrocytes mainly at tumor margins and showed enrichment of transcripts encoding the fatty-acid uptake protein cluster of differentiation 36 (CD36) in tumor regions [69]. These observations prompted functional tests of lipid synthesis in the proposed donor cells and of lipid uptake in recipient cells. In co-culture, FASN knockdown in MO3.13 oligodendrocytes or CD36 knockdown in recipient tumor or microglial cells attenuated tumor proliferation or the induction of immunosuppression-associated markers. Co-injection of FASN-silenced MO3.13 cells with H2030-BM cells also reduced brain metastatic burden [69]. Together, the spatial localization and perturbation results support a model in which oligodendrocyte lipid synthesis and recipient-cell uptake contribute to tumor-immune interactions. Direct in vivo tracing of lipid transfer would be needed to establish this donor-recipient relationship more firmly.

Experiments using astrocyte-conditioned medium and genetic perturbations suggest that tumor genotype can influence how BrM cells use host-derived fatty acids. In breast-cancer BrM models, p53 inactivation increased stearoyl-CoA desaturase 1 (SCD1), which converts saturated fatty acyl-CoAs into monounsaturated forms. SCD1 knockout counteracted the growth-promoting effects of p53 loss, which links this genotype to a requirement for fatty-acid desaturation [70]. Astrocyte-conditioned medium also promoted the proliferation of p53-deficient breast-cancer cells, and CD36-mediated fatty-acid uptake contributed to this proliferative effect [70]. These findings suggest that tumor-cell responses to astrocyte-derived lipids may involve both lipid uptake and intracellular processing. Beyond serving as substrates, astrocyte-derived fatty acids can influence tumor growth through signaling. In breast-cancer and melanoma BrM models, arachidonic and mead acids released by astrocytes activated the lipid-responsive transcription factor peroxisome proliferator-activated receptor γ (PPARγ) and promoted tumor-cell proliferation. PPARγ inhibition reduced brain metastatic burden, which supports a role for this signaling pathway in those models [71]. Thus, astrocyte-associated lipid metabolism may support growth through distinct processes, although their spatial distribution and relative contributions within human BrMs remain to be determined.

Together, these studies suggest that lipid metabolism supports BrM growth through several processes rather than simply through lipid accumulation. FASN-dependent synthesis contributes to brain tumor growth in HER2-amplified breast-cancer and NSCLC models, whereas studies of astrocyte-derived fatty acids implicate uptake and lipid-responsive signaling in additional growth-supporting mechanisms. The contrasting effects of FABP7 knockdown on lipid storage, oxidation, and intracranial growth further indicate that these metabolic processes should not be treated as interchangeable. Spatial imaging reveals regional lipid enrichment and isotope incorporation, and integrated spatial and functional analyses implicate oligodendrocytes as potential local lipid suppliers. It remains unresolved how tumor-cell synthesis, host-derived supply, and intracellular lipid use are coordinated within individual human BrMs, and whether the resulting dependencies recur across tumor lineages.

4.4. Mitochondrial Adaptation and Oxidative Phosphorylation

Mitochondrial adaptation in BrMs involves respiratory metabolism, biosynthetic support, and interactions with host cells [72,73]. These functions vary among the models examined [9]. Spatial studies help resolve where mitochondrial programs occur, whereas complementary functional experiments examine how they contribute to growth.

The regional glycolytic-OXPHOS contrast described in Section 4.1 provides an initial example of spatial variation in mitochondrial-associated programs within BrMs [12]. In a larger proteogenomic atlas, spatial transcriptomics of 12 BrMs and four matched primary tumors identified OXPHOS and nucleotide-biosynthesis enrichment in two malignant-cell-rich molecular niches, MN4 and MN9 [74]. These findings link oxidative transcriptional programs to regional cell composition. Spatial proteomic analysis of a melanoma patient further revealed higher mitochondrial and glycolytic protein abundance in one primary-tumour region than in another, with similar features observed in lung and brain metastases [75]. Thus, some mitochondrial-associated states may already occur within the primary tumor, although this retrospective comparison does not establish their clonal origin or respiratory activity.

Regional oxygen availability provides important physiological context for interpreting these molecular maps. In nude rats with stereotactically implanted H2030-BrM3 lung-cancer lesions, cortical tumors were larger and showed stronger hypoxia- and oxidative-stress-associated signals than striatal tumors, as assessed by proteomics, histology, and copper-64-labeled copper(II) diacetyl-bis(N^4-methylthiosemicarbazone) ([^{64}Cu]Cu-ATSM) PET [76]. Related work combined CA-IX staining in human NSCLC BrMs with rat imaging and documented regional oxygen heterogeneity in the model [77]. Oxygen supply could therefore influence the expression and function of respiratory pathways, but the accompanying difference in tumor size prevents attributing the effect to brain region alone. These measurements provide oxygenation context rather than regional OXPHOS flux.

Cellular composition is also important when assigning mitochondrial programs to specific tissue regions. GeoMx profiling of 44 NSCLC patients distinguished tumor, immune, and adjacent-brain compartments with distinct immune and fibrotic programs [11]. Although this study did not measure regional respiration directly, functional evidence highlights the importance of investigating the metabolic activity of neighboring myeloid cells. In experimental and human BrMs, tissue staining localized the macrophage migration inhibitory factor (MIF) receptor cluster of differentiation 74 (CD74) to microglia/macrophages, and experiments implicated tumor-derived MIF in their reprogramming. Bulk RNA sequencing of sorted mouse CD74-positive cells showed OXPHOS enrichment, and conditional deletion of the mitochondrial quality-control protease Oma1 in C-C chemokine receptor 2 (CCR2)-lineage cells reduced the brain tumor burden in a melanoma BrM mouse model without reducing the number of CD74-positive cells [78]. These results link myeloid mitochondrial regulation to tumor support rather than simply to myeloid-cell accumulation.

Spatial and functional studies also link mitochondrial remodeling in tumor cells to their interactions with the brain microenvironment. In TNBC mouse tumors, DSP identified immune changes that were associated with signal regulatory protein α (SIRPα)-regulated fibronectin. Complementary experiments linked fibronectin to microglial tolerance and tumor-cell SIRPα signaling through SH2 domain-containing protein tyrosine phosphatase 2 (SHP2) and ERK to mitochondrial fission mediated by dynamin-related protein 1 (DRP1), a regulator of mitochondrial division [79]. In LUAD BrM models, a separate study linked the neuropeptide VGF to mitochondrial fusion. VGF limited ABHD12B-mediated degradation of cardiolipin, a phospholipid that supports mitochondrial membrane organization, thereby favoring mitochondrial fusion and oxidative metabolism. Deletion of the VGF N-terminal domain impaired these processes and reduced brain colonization in mice [80]. Together, these studies suggest that both mitochondrial fission and fusion can support brain metastatic growth in the respective TNBC and LUAD models. It remains unclear whether the difference between these models reflects tumor origin, genotype, or experimental conditions.

Functional studies in TNBC BrM models suggest that nutrient availability shapes how mitochondrial metabolism supports tumor growth. CRISPR screening, isotope tracing, and respiratory assays identified the complex I subunit NADH: ubiquinone oxidoreductase subunit B9 (NDUFB9) as important under low-asparagine conditions. NDUFB9 knockout reduced intracellular aspartate production, whereas low asparagine increased asparagine synthetase expression, which drew on the remaining aspartate pool to sustain asparagine synthesis. Together, these effects limited the aspartate available for nucleotide biosynthesis and restricted brain tumor outgrowth [81]. These findings link respiratory-chain function to the supply of biosynthetic precursors rather than to adenosine triphosphate (ATP) production alone, and they raise the question of whether regional differences in asparagine availability influence the sensitivity of BrMs to NDUFB9 loss.

Broader cohort comparisons place these local observations in context. Bulk multi-omics across breast, lung, and renal cancers showed higher OXPHOS gene-set scores in BrMs than in matched primary or extracranial specimens [82]. Earlier breast-cancer analyses found enrichment relative to unmatched primary tumors but not relative to extracranial metastases, whereas separate oligomycin experiments were confined to conventional

2026, Vol. 3, Article ID. 2026.0030
https://doi.org/10.69709/GenomC.2026.133666

MDA-MB-231 cell assays [83]. The choice of comparison tissue therefore matters when interpreting apparent brain-associated enrichment. An OXPHOS-enriched epithelial transcriptional state projected onto primary-lung spatial sections [84] and a dissociated pan-cancer BrM atlas [85] provide complementary comparisons, but neither supplies regional measurements within BrM tissue.

In melanoma, glutamine dependence can make oxidative tumor states susceptible to metabolic inhibition. RNA sequencing of 88 resected BrMs identified a High-OXPHOS subgroup that was associated with shorter post-craniotomy survival. The glutaminase inhibitor CB-839 reduced oxygen consumption in High-OXPHOS cells and prolonged survival in mice bearing mitogen-activated protein kinase (MAPK)-inhibitor-resistant intracranial xenografts, thereby linking glutamine metabolism to mitochondrial respiratory support [86]. In a separate B16-F10 intracranial model, metformin plus anti-programmed cell death protein 1 (PD-1) therapy prolonged survival versus control and metformin alone but not significantly versus anti-PD-1 alone [86]. A 2025 bioRxiv preprint provided genetic evidence through peroxisome proliferator-activated receptor γ coactivator 1α (PGC1α), a coactivator of mitochondrial biogenesis, and NADH: ubiquinone oxidoreductase subunit S4 (NDUFS4), a complex I subunit. PGC1α deletion reduced lung and brain metastatic incidence in an autochthonous melanoma model, whereas NDUFS4 deletion reduced metastatic burden in transplantation models [87]. These preclinical results implicate substrate use and mitochondrial machinery at different stages of metastatic growth.

In lung cancer, mitochondrial-associated states can also accompany changes in the immune environment. Bulk and single-cell multi-omics linked BrMs to mitochondrial-pathway enrichment and reduced immune programs. Gamitrinib, which targets mitochondrial heat shock protein 90 (Hsp90)-dependent protein homeostasis, showed activity in 20 BrM-derived organoid models. Combined with anti-PD-1 therapy, it prolonged survival compared with control in an LLC-Luc mouse BrM model but not significantly versus either monotherapy [88]. This supports further testing of mitochondrial targeting, but does not establish an advantage over monotherapy. Lung-cancer BrMs are also not metabolically uniform. Transcriptomic comparisons found relatively greater glycolytic programs in hepatocyte growth factor receptor (MET)-amplified LUAD BrMs and oxidative programs in MET-wild-type BrMs [89], which suggests that molecular subtype may help to interpret the mitochondrial states identified by spatial profiling.

Together, these studies suggest that mitochondrial adaptation supports BrM growth through context-dependent functions in both tumor and host cells. Spatial analyses locate oxidative transcriptional programs and mitochondrial-associated protein patterns, whereas functional studies implicate glutamine-supported respiration, aspartate-dependent biosynthesis, and mitochondrial remodeling. Their convergence lies in mitochondrial involvement rather than in a single shared respiratory dependency. Linking these functions to defined cells and regions could clarify how nutrient supply, tumor genotype, and immune composition influence mitochondrial vulnerabilities within individual BrMs.

4.5. Shared, Lineage-Associated, and Brain-Site-Associated Programs

Across breast-cancer, lung-cancer, and melanoma BrMs, recurring features include altered substrate use, lipid handling, and mitochondrial support for growth, although the mechanisms regulating these processes vary. For example, fatty-acid synthesis can support growth in both breast-cancer and NSCLC BrM models [63,65]. Pan-cancer profiling also identifies molecular states that extend across primary-tumor origins [74], which suggests that lineage alone does not explain BrM metabolic heterogeneity. These findings support convergence on related metabolic functions rather than identical dependencies. Conversely, a mechanism that has been studied in only one lineage cannot yet be considered specific to that lineage.

Brain-site adaptation is more convincingly supported when functional dependence differs between anatomical sites. Greater sensitivity to FASN disruption in brain tumors than in mammary-fat-pad or liver tumors provides such support in HER2-amplified breast-cancer models [63]. Yet a metabolic state detected in BrMs need not have arisen in the brain. In the melanoma case discussed in Section 4.4, related glycolytic and mitochondrial protein features were already detectable in the primary tumor [75]. Such pre-existing variation, together with selection, local induction, and treatment, may shape the metastatic state. Matched primary and extracranial comparisons help distinguish these possibilities, but functional or temporal evidence is needed to determine how such states arise. Therapeutic prioritization should therefore consider tumor origin together with molecular state and local metabolic context. Candidate metabolism-directed interventions are summarized in Table 1.

Table 1: Candidate metabolism-directed interventions relevant to BrMs: evidence base, clinical status, and limitations.

Inhibitor/ Intervention	Target/Mechanism of Action	Metabolic Axis	Evidence and Limitations	Development Status
Telaglenastat (CB-839)	GLS1 inhibition	Glutamine-supported anaplerosis and respiration	CB-839 reduced respiration in high-OXPHOS melanoma cells and prolonged survival in established A375-R1 and MEL624 intracranial xenografts [86]. Systemic trials evaluated GLS1 inhibition and tolerability [90,91].	Phase I monotherapy was completed. The nivolumab combination trial was stopped for insufficient efficacy (NCT02771626); no dedicated BrM efficacy cohort.
GABA uptake inhibitors Tiagabine; NO-711	GABA transporter inhibition	GABA-shunt substrate uptake	Both agents suppressed brain metastatic progression in nicotine-associated lung-cancer mouse models, supporting GABA uptake as an experimental therapeutic target [61].	Tiagabine is approved as adjunctive therapy for partial seizures but not for BrMs. NO-711 is a research compound.
FASN inhibitors BI99179; TVB-2640 (denifanstat)	FASN inhibition	De novo fatty-acid synthesis	BI99179 inhibited HER2-positive breast tumor growth in the brain but not in the mammary fat pad [63]. TVB-2640 reduced the outgrowth and invasion of TNBC BrM-related cells and acted synergistically with free SN-38 in vitro [92]. The NSCLC spatial/NET study did not establish intracranial TVB-2640 efficacy because its A549 model lacked clear BrMs [68].	BI99179 remains preclinical. Denifanstat phase II trials in astrocytoma and HER2-positive metastatic breast cancer have been completed (NCT03032484; NCT03179904), with results reported but without a dedicated BrM efficacy evaluation.
SCD1 inhibitor SW203668	SCD1 inhibition	Fatty-acid desaturation	In human breast-BrM organotypic cultures, SW203668 increased apoptosis ($n = 3$); reduced Ki67 (antigen Ki-67, a proliferation marker) expression was a nonsignificant trend ($n = 5$). These are ex vivo responses and do not demonstrate patient efficacy [70].	Experimental compound; clinical BrM efficacy and tolerability have not been established.
ACSS2 inhibitors AD-5584; AD-8007	ACSS2 inhibition	Acetate-to-acetyl-CoA conversion	Both compounds showed brain exposure in mice and activity in ex vivo breast-BrM slices. AD-8007 reduced intracranial burden and prolonged survival; AD-5584 suppressed BrM growth through a ferroptosis-associated mechanism [47,48].	Preclinical leads; human dosing and efficacy have not been established.
PHGDH inhibitors PH-719; PH-755	PHGDH inhibition	Serine/glycine synthesis	Serine/glycine restriction sensitized TNBC, melanoma, and ccRCC BrM cells in culture. PH-755 reduced established TNBC/ccRCC intracranial tumors and prolonged survival in a separate preventive TNBC experiment. Glucose tracing and hyperpolarized pyruvate imaging provided metabolic readouts [49].	Preclinical BrM studies; no established clinical use.

2026, Vol. 3, Article ID. 2026.0030
https://doi.org/10.69709/GenomC.2026.133666

Table 1: *Cont.*

Inhibitor/ Intervention	Target/Mechanism of Action	Metabolic Axis	Evidence and Limitations	Development Status
IACS-010759	Complex I inhibition	OXPHOS	Treatment prolonged survival in intracranial melanoma xenografts and reduced BrM incidence in a spontaneous model [93]. In the breast-cancer experiment, dosing began before tumor-cell inoculation, supporting prevention rather than established-lesion treatment [82].	Phase I development was limited by elevated lactate levels and neurotoxicity; no recommended phase II dose was established [94] (NCT03291938).
Metformin	Pleiotropic biguanide; indirect complex I inhibition	Respiration and immune signaling	In intracranial B16-F10 melanoma tumors, metformin increased immune-activation transcripts. Metformin plus anti-PD-1 improved survival versus control and metformin alone but not significantly versus anti-PD-1 alone [86].	Approved for type 2 diabetes; use in BrM treatment remains investigational.
DRP1 depletion/mdivi-1	Genetic DRP1 depletion; pharmacological tool	Mitochondrial dynamics and FAO	DRP1 depletion and mdivi-1 reduced intracranial burden in HER2-positive breast-cancer models [95]. Genetic evidence supports a role for DRP1, but mdivi-1 also inhibits complex I independently of DRP1 [96].	Preclinical BrM evidence; mdivi-1 shows limited target specificity.
Gamitrinib	Mitochondrial Hsp90/TRAP1 inhibition	Mitochondrial protein homeostasis	Induced apoptosis in lung-BrM patient-derived organoids and prolonged mouse survival as monotherapy. Adding anti-PD-1 was not significantly superior to either agent alone [88].	Phase I trial in advanced cancers, listed in the registry as recruiting (NCT04827810); no BrM-specific clinical efficacy reported.
L-arginine	NO-linked metabolic modulation; hypothesized radiosensitization	Arginine/NO and lactate metabolism	A 63-patient randomized BrM study reported improved response and CNS control with oral L-arginine plus twice-daily whole-brain radiotherapy and a boost [97]. An intravenous study (n = 20) showed acute MRS lactate/creatine changes but not efficacy or an optimal dose [98].	Investigational radiosensitization; the small trial and radiation schedule limit generalizability. An early phase I BrM trial is listed in the registry as recruiting (NCT06328686).
Ketogenic diet	Carbohydrate restriction to induce ketosis	Systemic glucose/ketone availability	The cited NSCLC-BrM case began dietary treatment after chemoradiotherapy and was later stopped because of dyslipidemia; benefit cannot be attributed to diet alone [99].	Investigational. NCT05428852 is suspended; NCT05564949 is listed in the registry as recruiting. Neither has posted results.
MCT1 inhibitors AR-C117977; AZD3965	MCT1 inhibition	Lactate/pyruvate transport	AR-C117977 reduced glioblastoma stem-like cell viability in vitro; neither a BrM model nor a tumor-stromal lactate-transfer experiment was included [100].	AZD3965, a different compound, completed a phase I trial in advanced cancers (NCT01791595); no dedicated BrM efficacy analysis.

Table 1: *Cont.*

Inhibitor/ Intervention	Target/Mechanism of Action	Metabolic Axis	Evidence and Limitations	Development Status
JHU-083	Prodrug of glutamine antagonist DON	Glutamine-dependent biosynthesis	Oral JHU-083 produced measurable brain exposure to active DON in mice; antitumor activity was reported in medulloblastoma and orthotopic glioma but not in BrMs [101–103].	Preclinical evidence from primary CNS and extracranial tumors; no clinical BrM data are available.
Etomoxir	CPT1-directed tool compound	Fatty-acid oxidation	Glioma cultures and orthotopic models showed growth inhibition [104,105]. High concentrations (including 100 μM) and off-target effects limit the attribution to CPT1-dependent FAO [106].	Laboratory probe; no established BrM application.
Devimistat (CPI-613)	Lipoate analogue affecting PDH and α-KGDH	TCA-cycle metabolism	TCA-cycle perturbation was shown in non-BrM carcinoma cells and xenografts; direct BrM efficacy and brain exposure were not reported [107].	No BrM trial has been reported. Phase III AVENGER 500 did not improve survival in pancreatic cancer [108] (NCT03504423).

Evidence is specific to the compound, tumor origin, and experimental setting examined; the final four entries provide indirect evidence from non-BrM models. Intracranial implantation tests brain tumor growth but bypasses metastatic dissemination. Clinical status refers to the named compound and indication, rather than to proven BrM efficacy; registry status was checked on 13 September 2026 and may lag behind actual recruitment.

5. Translational Implications of Spatially Resolved Metabolism

5.1. From Spatial Vulnerability to Therapeutic Prioritization

Spatially resolved metabolism can help prioritize therapeutic hypotheses by showing where candidate vulnerabilities arise within BrMs. Vascular, fibrotic, glial, and immune regions contain distinct malignant and microenvironmental programs [11], which provide tissue context for the metabolic mechanisms discussed in Section 4. Relating these states to tumor origin and treatment history may guide target selection and the development of tissue or imaging assays [9,109]. Table 1 summarizes candidate interventions that target glycolysis, glutamine metabolism, lipid synthesis, and OXPHOS.

The translational path depends on whether a spatial finding is developed as a therapeutic target or as a biomarker. For a candidate target, regional RNA or protein enrichment should be linked to metabolic function and tested for selective dependence through genetic or pharmacological perturbation, with attention to brain drug exposure and effects on surrounding brain tissue (Figure 2). A biomarker need not itself cause the phenotype it predicts, and correlation alone does not establish a causal role. Instead, its validation should begin with a defined diagnostic, monitoring, or treatment-selection use, followed by demonstration of analytical reliability and independent clinical validation in the intended population [110]. If a biomarker is to guide treatment, evidence is also needed that acting on its result improves decisions or outcomes beyond existing clinical assessment. Spatial discovery can inform both routes, but it does not by itself establish clinical utility.

5.2. Niche-Linked Metabolic Targeting and the Bridge to Imaging

Mitochondrial inhibition illustrates how recurrent metabolic features can inform therapeutic strategies without yet defining a biomarker for patient selection. In lung-cancer BrMs, multi-omic analysis linked a mitochondrial-high state to preclinical gamitrinib sensitivity [88], whereas melanoma and lung-cancer studies linked OXPHOS-related programs to aggressive behavior or sensitivity to mitochondrial inhibition in experimental models [9,86,88]. Together with the regional oxidative programs discussed in Section 4.4, these results support testing whether the mapped states identify drug-sensitive tumor regions. However, they do not yet show that an OXPHOS-high region in a patient is selectively dependent on that pathway.

2026, Vol. 3, Article ID. 2026.0030
https://doi.org/10.69709/GenomC.2026.133666

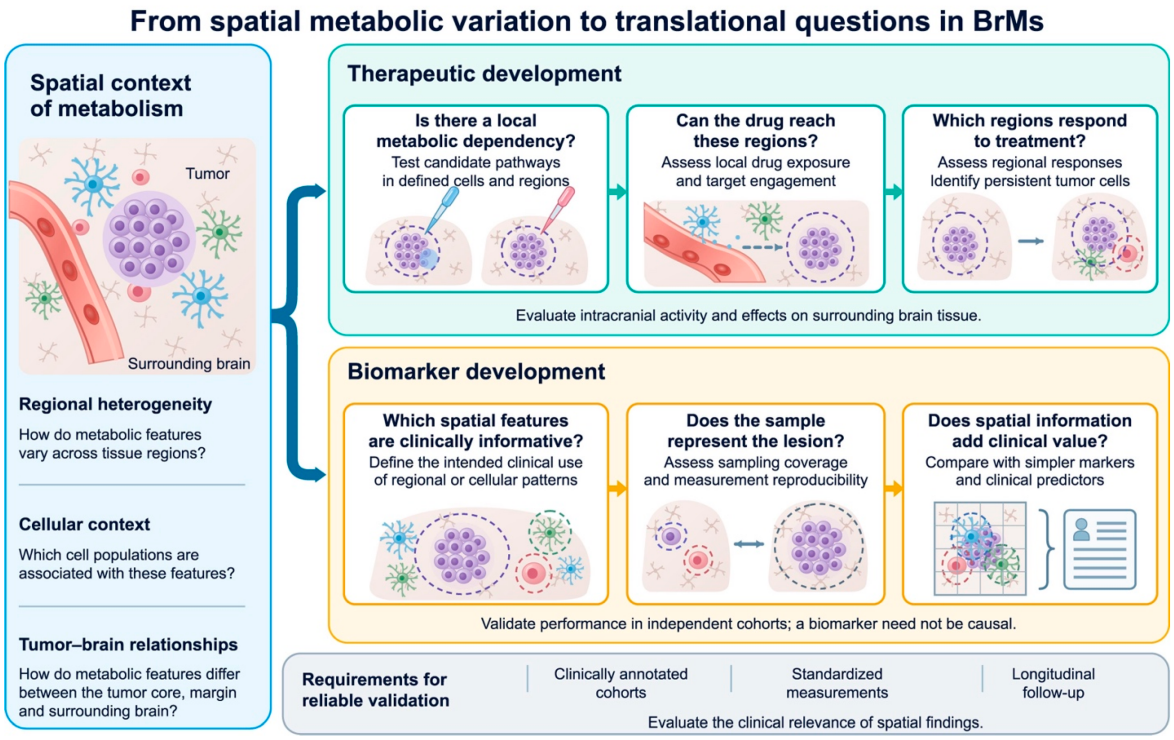

Figure 2: Spatial metabolic heterogeneity and translational development in BrMs. Spatial findings are interpreted within their regional and cellular contexts, including the tumor core, margin, and surrounding brain. The upper pathway outlines therapeutic development, proceeding through tests of local metabolic dependency, drug exposure, and target engagement, followed by evaluation of regional treatment responses and of effects on surrounding brain tissue. The lower pathway outlines biomarker development, emphasizing the intended clinical use, sampling coverage, measurement reproducibility, and added value over simpler markers and clinical predictors. Biomarkers require validation in independent cohorts but need not be causal. Clinically annotated cohorts, standardized measurements, and longitudinal follow-up support both routes. The schematic presents questions for investigation rather than established clinical applications. BrMs, brain metastases.

Fatty-acid synthesis and host-derived lipid signaling provide a second set of therapeutic hypotheses. Breast-cancer BrM models support both FASN-dependent synthesis and growth responses to astrocyte-derived polyunsaturated fatty acids [63,71]. In TNBC brain-tropic and BrM-derived cell lines, TVB-2640 reduced spheroid outgrowth, migration, and invasion and acted synergistically with SN-38 in three-dimensional assays, but no in vivo test of BrM efficacy was performed [92]. In human NSCLC BrM tissue, integrated spatial analyses linked palmitate enrichment to neutrophil-rich regions and EMT-related programs [68]. These observations, together with separate FASN-inhibition experiments, support further investigation of this pathway, although the NSCLC animal model did not establish intracranial efficacy. Across these studies, regional lipid enrichment has not been validated as a predictor of response to FASN inhibition.

Serine biosynthesis and glutamate-centered neurometabolic coupling represent additional preclinical therapeutic targets [49,55,56]. Because these dependencies were largely established through tracing, cell-based assays, or animal experiments, spatial analysis could help determine where they are relevant in human lesions and whether their distribution varies with tumor origin or treatment. Such comparisons could inform future studies on treatment stratification without assuming that a mechanism observed in one model is shared by all BrMs.

Clinical evaluation of these strategies remains at an early stage. Gamitrinib has entered a phase I trial in advanced cancers (NCT04827810), whereas TVB-2640 (denifanstat) was evaluated with bevacizumab in recurrent high-grade astrocytoma rather than specifically in BrMs (NCT03032484). Registered ketogenic-diet studies include patients with BrMs (NCT05428852; NCT05564949) and address feasibility or clinical outcomes rather than selection by a spatial metabolic signature. The next translational step is to link a defined intervention to a measurable patient state and an appropriate intracranial endpoint.

Imaging offers a complementary route to translation by tracking lesion features that cannot be sampled repeatedly. In lung-derived BrM models, oxygen-

enhanced imaging localized hypoxia, and radiotherapy guided by hypoxia imaging improved tumor control and animal survival [77]. This provides a preclinical example of a regional physiological measurement informing treatment. In patients, amino-acid PET has a more developed framework for acquisition and response assessment, provided by the joint guideline from the European Association of Nuclear Medicine (EANM), European Association of Neuro-Oncology (EANO), Response Assessment in Neuro-Oncology (RANO) working group, and Society of Nuclear Medicine and Molecular Imaging (SNMMI) and by the PET RANO BM 1.0 criteria [111,112]. Serial uptake measurements can complement MRI assessment [111], as illustrated by longitudinal O-(2-[^{18}F]fluoroethyl)-L-tyrosine (^{18}F-FET) PET studies in melanoma- and lung-cancer BrMs [113]. The PURSUE study addressed the more specific problem of distinguishing recurrence from treatment-related change after radiotherapy. Among 23 patients with MRI-indeterminate lesions and histopathological verification, an ^{18}F-fluciclovine maximum standardized uptake value (SUVmax) threshold derived in the study yielded 80% sensitivity and 85% specificity [114]. *The threshold* requires independent validation beyond this small, surgically selected cohort; the study did not show that PET-guided management improves outcomes.

Delayed glucose-tracer imaging illustrates both the potential and the limitations of an additional diagnostic readout. In a retrospective series of 34 irradiated BrM patients, a delayed 2-deoxy-2-[^{18}F]fluoro-D-glucose (^{18}F-FDG) tumor-to-background SUVmax ratio threshold yielded 94.1% specificity but 58.8% sensitivity for recurrent disease [115]. No individual PET metric outperformed MRI overall; only ten patients had histopathological verification, and the threshold was derived from the same cohort. Delayed FDG-PET may therefore provide supplementary information in selected indeterminate cases rather than replace MRI or establish a tissue-level metabolic dependency.

Magnetic resonance spectroscopy (MRS) can address a different translational question by measuring localized metabolic responses to an intervention. In a randomized 20-patient pharmacodynamic study, serial single-voxel ^{1}H-MRS showed a decrease in the lactate-to-creatine peak-area ratio after intravenous L-arginine compared with saline. The largest descriptive median reduction occurred in the 30-g group, but baseline imbalance limited the dose comparisons, and the five patients per group with single-dose follow-up supported feasibility rather than therapeutic efficacy [98]. Such measurements could provide pharmacodynamic readouts alongside tissue-derived hypotheses, although a change in a metabolite ratio does not directly measure flux.

A longitudinal study could link tissue discovery to these clinical readouts, starting at the first clinically indicated BrM resection. Co-registering a spatial map with MRI and, where available, amino-acid PET would allow candidate tissue states to be related to imaging features and cerebrospinal fluid (CSF) or plasma analytes. Serial imaging and liquid biopsy, with CSF collected when clinically indicated, could then be used to follow treatment; repeat tissue would be collected only at clinically indicated re-resection or autopsy. Existing liquid-biopsy studies show why the sampling compartment matters. In 92 patients with newly diagnosed NSCLC BrMs, an early decrease in CSF circulating tumor DNA (ctDNA) tracked intracranial response more closely than did plasma, whereas plasma ctDNA was undetectable in all 13 patients with intracranial-only melanoma in a separate cohort [116,117]. These findings support CNS-aware monitoring, but serial ctDNA changes have not yet been linked to specific spatial metabolic states. That relationship, as well as the added value of CSF or plasma metabolomics, would need to be tested prospectively.

5.3. Spatial Niche States as Candidate Biomarkers

Spatial immune features and metabolism-associated tissue states represent different kinds of biomarker candidates. Some are associated with treatment response or survival, whereas others primarily identify regions in which a metabolic mechanism could be investigated. Distinguishing these uses helps to avoid treating an immune neighborhood, an enzyme-expression signal, and a validated metabolic readout as equivalent.

Clinical studies increasingly support considering immune-cell arrangement alongside phenotype. Human BrM imaging and tissue analyses linked highly invasive, immune-cold lesions to chitinase-3-like protein 1 (CHI3L1), with complementary experiments supporting a role for CHI3L1 in the immune phenotype [35]. In melanoma BrMs, clustered T-cell infiltration was associated with response to immune checkpoint blockade and with survival [118]. These findings suggest that the spatial organization of immune cells and the invasive interface may carry clinically relevant information, although neither constitutes a metabolic biomarker itself.

Macrophage studies further show why cell identity and spatial location should be considered together. IMC in treatment-naive breast-cancer BrMs identified a cluster of differentiation 163 (CD163)-positive macrophage-exhausted T-cell neighborhood associated with immune

2026, Vol. 3, Article ID. 2026.0030
https://doi.org/10.69709/GenomC.2026.133666

escape [119]. By contrast, spatial and single-nucleus profiling across lung-, breast-, and melanoma-derived BrMs linked tumor-contacting human leukocyte antigen DR (HLA-DR)-positive inflammatory macrophages to treatment responsiveness and longer survival, whereas macrophages associated with extracellular matrix (ECM) and transforming growth factor β1 (TGFβ1) programs were associated with poorer outcomes [120]. These studies support evaluating specific macrophage states rather than interpreting macrophage abundance uniformly. The distinct populations and endpoints across these studies do not establish a common metabolic biomarker across tumor origins.

In experimental BrMs, spatial profiling can also be combined with perturbation to test immune mechanisms. In a breast-cancer BrM mouse model, spatial transcriptomics localized arginase 1 (ARG1)-positive macrophages to the invasive edge; tumor-cell interleukin 34 (IL34) deletion prevented cerebellar tumor establishment, and colony-stimulating factor 1 receptor (CSF1R) blockade reduced tumor growth, whereas human tissue supported IL34 expression [121]. This links a spatially localized macrophage state to a targetable signaling pathway in the model but does not establish regional arginine flux or validate IL34/ARG1 as a clinical response assay.

Metabolism-associated immune states remain less directly linked to clinical decisions. In LUAD BrMs, integrated multi-omic analysis linked glycolytic signatures and lactate-related remodeling to reduced cytotoxic immune features and immunosuppressive programs [43]. This provides a rationale to test whether a glycolytic-immune state is associated with treatment response.

Tryptophan-catabolic programs illustrate how spatial data can refine such hypotheses. GeoMx profiling of NSCLC primary tumors and BrMs identified reduced antigen-presentation and lymphocyte programs in the brain metastatic microenvironment [11]. Within tumor-adjacent brain, interleukin-4-induced protein 1 (IL4I1) expression was higher than in control brain, whereas indoleamine 2,3-dioxygenases 1 and 2 (IDO1/IDO2) and tryptophan 2,3-dioxygenase 2 (TDO2) were higher in nonfibrotic than highly fibrotic regions. Given the immunoregulatory role of tryptophan-derived aryl hydrocarbon receptor (AHR) ligands [11,122], these RNA-level differences point to a locally variable mechanism rather than demonstrate increased pathway activity. The same NSCLC analysis linked highly fibrotic tumor-adjacent regions to greater inferred M2 (alternatively activated) macrophage abundance and hypoxia-related programs, whereas nonfibrotic regions showed greater inferred cluster of differentiation 8 (CD8)-positive T-cell abundance [11]. Fibrosis may therefore help define the cellular context in which tryptophan-catabolic signals are interpreted, but neither the enzyme-expression pattern nor the immune-fibrotic state has been validated as a treatment-response biomarker.

Vascular organization may provide another context for metabolism-associated immune variation. In gastric-cancer BrMs, angiogenic and vessel-co-opting regions differed in their immune composition and in features related to oxidized nicotinamide adenine dinucleotide (NAD+), including nicotinamide phosphoribosyltransferase (NAMPT) expression [13]. This links a candidate metabolic signal to vascular and cellular context, without measuring regional NAD+ turnover. Similarly, Visium profiling of mouse BrM sections identified enrichment of translation, ribosomal, and selenoamino-acid-metabolism pathways in thalamic S1 regions, defined as tumor-surrounding spots within approximately 105 μm of the tumor border [123]. Such maps can nominate regional features for biomarker evaluation, although their associations with treatment response and patient outcomes require further investigation.

Clinical development should therefore begin with the clinical decision that a candidate marker is intended to inform. An assay proposed to predict treatment benefit should distinguish response to a specified therapy from general prognosis. A monitoring assay should add useful information to serial MRI and established response assessment, and a recurrence classifier should be tested against pathology, where available, and against rigorous follow-up. Single markers and composite spatial signatures are both legitimate candidates; the latter should demonstrate added value beyond simpler assays, tumor origin, treatment history, and other relevant clinical predictors. Independent validation in the intended setting, followed by evaluation of how the result changes management, is more informative than requiring that every biomarker describe an entire niche.

6. Challenges and Future Directions

Clinical access determines which BrMs are available for study, and tissue handling and preservation influence how accurately measurements reflect their metabolic state. Most specimens come from surgically accessible, clinically advanced, symptomatic, or treatment-exposed lesions, which leaves early colonization, micrometastatic states, and dormant states underrepresented [12,74,85]. Cold ischemia, handling, and preservation can also alter labile metabolites [124], and interactions with metabolically responsive host cells add to the biological complexity [10]. Differences between tissue maps may therefore

reflect disease stage and sample processing as well as tumor biology.

Combining complementary tissue sources could help address this sampling bias, whereas imaging and clinically indicated CSF profiling could provide longitudinal monitoring. The first clinically indicated BrM resection can provide a useful sampling point, although it is not necessarily early in colonization or before treatment. Matched primary, extracranial-metastasis, and BrM tissue can inform evolutionary relationships and site-associated programs, whereas rapid-autopsy collections can capture microscopic foci; however, these cross-sectional designs do not track occult colonization or dormancy within the same patient [82,125,126]. For example, rapid-autopsy tissue from two patients with TNBC and two with HER2-positive breast cancer contained microscopic brain metastases with perivascular or spheroidal growth patterns, thereby extending anatomical observations beyond surgically resected macrometastases [127]. Combining surgical and autopsy collections across centers could broaden the disease states represented, and treatment histories could help interpret differences between samples. Serial imaging or clinically indicated CSF profiling can extend follow-up to unresected lesions, without requiring research-only biopsy of small, deep, or eloquent-region lesions.

When repeat tissue sampling is clinically indicated, spatial analysis can add a temporal dimension to these comparisons. A cohort of patients with metastatic TNBC and extracranial disease illustrates the value of comparing primary, pretreatment metastatic, and on-treatment specimens [128]. In BrMs, such opportunities are more restricted and should be linked to the imaging and liquid-biopsy follow-up outlined in Section 5.2. Such follow-up can track disease change between tissue collections but does not reconstruct the intervening spatial metabolic states.

The central technical challenge is to link a regional molecular pattern to metabolic function. Enzyme regulation can uncouple transcript abundance from activity [17, 129], and protein localization does not eliminate this distinction [130,131]. Metabolite imaging and single-cell metabolomics provide complementary chemical measurements [132], with increasing molecular coverage [133], but static abundance alone still cannot establish pathway activity [9,133]. A claim of metabolic dependency requires selective perturbation linked to a relevant functional outcome, with controls for off-target effects. Flux estimation requires tracer design and quantitative interpretation appropriate to the pathway, including consideration of tracer availability, labeling time, and metabolite pool sizes; isotope labeling alone does not establish quantitative flux [134].

The studies reviewed in Section 4 provide a starting point for this validation. Bulk metabolite profiles of BrMs [74], spatial lipid maps [67,68], melanoma substrate-tracing experiments [93], and complementary tracing or perturbation studies in human brain tumors and BrM models of breast cancer and melanoma each address a different part of the problem [46,63,87]. Isotope-resolved imaging and tissue-slice tracing in other tumors provide additional experimental approaches [135,136]. Notably, intraoperative glucose tracing with DESI-MSI resolved regional labeling in one human BrM [38]. The next priority is to reproduce such measurements across patients, accounting for tissue composition and tracer delivery. Model studies can then help test the functional significance of substrate use, as illustrated by the respiratory and biosynthetic role of NDUFB9 [81], without assuming that the same dependency has already been established in the mapped human regions.

Assigning metabolic activity to its cellular source is especially important in the brain, where tumor cells coexist with metabolically active neural, glial, and vascular cells. A key question is whether metabolites detected in tumor regions are synthesized by tumor cells or taken up from the surrounding tissue. Isotope tracing can help assess substrate contributions and metabolic fate [134] and could be combined with cell-type-resolved localization and selective perturbation in experimental models to distinguish between these alternatives. For a proposed donor-recipient interaction, disrupting synthesis in the candidate donor and uptake in the recipient, while measuring labeled metabolites and recipient function, would help distinguish local production from donor-derived supply. This design would test the proposed exchange rather than infer it from proximity.

Future technologies should be chosen based on the biological questions they are meant to resolve. Co-registering molecular measurements with histopathology can relate inferred pathways to measured metabolites and tissue composition [23,26,137,138]. Harmonized protocols and matched primary, extracranial, and BrM collections, analyzed by tumor origin, genotype, and treatment exposure, would make site-associated differences more interpretable [25,27,74]. Regional biochemical and imaging measurements can help prioritize questions for model-based tracing and perturbation [54,58]. Three-dimensional reconstruction or artificial intelligence (AI)-assisted alignment may improve integration, but their accuracy and uncertainty need evaluation in held-out samples. Subsequent clinical validation should follow the intended use of a target or biomarker, as discussed in Sec-

2026, Vol. 3, Article ID. 2026.0030
https://doi.org/10.69709/GenomC.2026.133666

tion 5 [109,112]. The immediate priorities are therefore comparable sampling, regional functional testing, and independent replication, rather than adding platforms without a defined biological or clinical question [139].

Cost and access will influence whether these designs can be reproduced beyond specialist centers. Discovery-scale spatial profiling remains expensive and computationally demanding, and differences in protocols and analyses impede cross-center comparison [139]. Shared cores could support discovery, and targeted panels or multiplex imaging could be used for replication if they retain the relevant biological information. Common reference materials, open analysis pipelines, and cross-center benchmarking could broaden participation without requiring every center to operate the full discovery workflow.

7. Conclusions

Spatial omics shifts the unit of analysis in BrMs from the average lesion to the local niche. Read alongside functional studies, these maps point to recurring roles for substrate use, lipid handling, and mitochondrial support of growth, rather than a single metabolic program shared by all BrMs. Similar functions can involve different molecular routes, with tumor genotype, neighboring cells, and local supply influencing their contribution. Spatial context therefore helps distinguish where a metabolite accumulates from which cells may produce, use, or respond to it. Likewise, a state observed in BrMs does not necessarily originate in the brain; pre-existing tumor features, selection during metastasis, and local or treatment-induced changes may all contribute. The next step is to determine which candidate metabolic processes sustain growth or immune suppression in the nominated regions and in which biological settings. For clinical translation, corresponding tissue or imaging readouts will also require independent validation for a defined purpose, such as treatment stratification or response monitoring. By locating candidate metabolic vulnerabilities within specific cellular and tissue contexts, spatial omics can help prioritize interventions for testing in the BrM settings most likely to depend on these processes.

List of Abbreviations

3PG	3-Phosphoglycerate
ABAT	4-Aminobutyrate Aminotransferase
ABHD12B	Abhydrolase Domain-containing Protein 12B
Acetyl-CoA	Acetyl-Coenzyme A
ACSS2	Acetyl-CoA Synthetase 2 (acyl-CoA synthetase short-chain family member 2)
ADP	Adenosine Diphosphate
AFADESI-MSI	Air-Flow-Assisted Desorption Electrospray Ionization Mass Spectrometry Imaging
AHR	Aryl Hydrocarbon Receptor
AI	Artificial Intelligence
ALKBH5	AlkB Homolog 5
ARG1	Arginase 1
ATP	Adenosine Triphosphate
BBB	Blood-Brain Barrier
BCAT1	Branched-Chain Amino-Acid Aminotransferase 1
BrM	Brain Metastasis
BrMs	Brain Metastases
BTB	Blood-Tumor Barrier
CA-IX	Carbonic Anhydrase IX
Cas9	CRISPR-Associated Protein 9
CCR2	C-C Chemokine Receptor 2
ccRCC	Clear-Cell Renal Cell Carcinoma
CD163	Cluster of Differentiation 163
CD36	Cluster of Differentiation 36
CD74	Cluster of Differentiation 74
CD8	Cluster of Differentiation 8
CHI3L1	Chitinase-3-Like Protein 1
CNS	Central Nervous System
CoA	Coenzyme A
CODEX	CO-Detection by indEXing
CPT1	Carnitine Palmitoyltransferase 1
CREB1	Cyclic Adenosine Monophosphate Response Element-Binding Protein 1
CRISPR	Clustered Regularly Interspaced Short Palindromic Repeats
CSF	Cerebrospinal Fluid
CSF1R	Colony-Stimulating Factor 1 Receptor
ctDNA	Circulating Tumor DNA
Cu-ATSM	Copper(II) Diacetyl-bis (N^4-Methylthiosemicarbazone)
Cyt c	Cytochrome c
DESI-MSI	Desorption Electrospray Ionization Mass Spectrometry Imaging
DGE-CEST	Dynamic Glucose-Enhanced Chemical Exchange Saturation Transfer
DON	6-Diazo-5-oxo-L-Norleucine
DRP1	Dynamin-Related Protein 1
DSP	Digital Spatial Profiling
EAAT1; EAAT2	Excitatory Amino-Acid Transporters 1 and 2
EANM	European Association of Nuclear Medicine
EANO	European Association of Neuro-Oncology
ECM	Extracellular Matrix

EGFR	Epidermal Growth Factor Receptor	MCT1	Monocarboxylate Transporter 1
EMT	Epithelial-Mesenchymal Transition	MERFISH	Multiplexed Error-Robust Fluorescence in Situ Hybridization
ERK	Extracellular Signal-Regulated Kinase		
FABP7	Fatty-Acid-Binding Protein 7	MIF	Macrophage Migration Inhibitory Factor
FAK	Focal Adhesion Kinase		
FAO	Fatty-Acid Oxidation	miR-199b-5p	MicroRNA-199b-5p
FASN	Fatty Acid Synthase	MET	MET Receptor Tyrosine Kinase (hepatocyte growth factor receptor)
FDG	2-Deoxy-2-fluoro-D-Glucose (^{18}F-labeled in PET)	mGluR1	Metabotropic Glutamate Receptor 1
FET	O-(2-Fluoroethyl)-L-Tyrosine (^{18}F-labeled in PET)	miR-32-3p	MicroRNA-32-3p
		MN	Molecular Niche (MN4 and MN9 are study-defined niche labels)
FOXA2	Forkhead Box A2		
G6P	Glucose-6-Phosphate	MRI	Magnetic Resonance Imaging
G6PD	Glucose-6-Phosphate Dehydrogenase (also termed G6PDH)	mRNA	Messenger RNA
		MRS	Magnetic Resonance Spectroscopy
GABA	γ-Aminobutyric Acid	MSI	Mass Spectrometry Imaging
GAD1	Glutamate Decarboxylase 1	mTOR	Mechanistic Target of Rapamycin
Gln	Glutamine	m^{6}A	N^6-Methyladenosine
Glu	Glutamate	NAD+	Oxidized Nicotinamide Adenine Dinucleotide
GLS1	Glutaminase 1		
Glx	Combined Glutamate-Glutamine Pool	NADH	Reduced Nicotinamide Adenine Dinucleotide
GluN2B	GluN2B Subunit of the NMDAR, Encoded by GRIN2B	NADPH	Reduced Nicotinamide Adenine Dinucleotide Phosphate
GRIN2B	Glutamate Ionotropic Receptor NMDA Type Subunit 2B (gene encoding GluN2B)	NAMPT	Nicotinamide Phosphoribosyltransferase
		NDUFB9	NADH:ubiquinone Oxidoreductase Subunit B9
H3K18la	Histone H3 Lysine 18 Lactylation	NDUFS4	NADH:ubiquinone Oxidoreductase Subunit S4
HER2	Human Epidermal Growth Factor Receptor 2	NET; NETs	Neutrophil Extracellular Trap; Neutrophil Extracellular Traps
HIF-1α	Hypoxia-Inducible Factor 1α		
HK2	Hexokinase 2	NF-κB	Nuclear Factor κB
HLA-DR	Human Leukocyte Antigen DR, a major histocompatibility complex class II molecule	NMDAR	N-Methyl-D-Aspartate Receptor
		NMR	Nuclear Magnetic Resonance
		NO	Nitric Oxide
Hsp90	Heat Shock Protein 90	NSCLC	Non-Small Cell Lung Cancer
IDO1; IDO2	Indoleamine 2,3-Dioxygenases 1 and 2	Oma1	Mouse Gene Encoding the Mitochondrial Metalloprotease OMA1
IGF2BP3	Insulin-like Growth Factor 2 Messenger RNA-Binding Protein 3	OXPHOS	Oxidative Phosphorylation
		p53	Tumor Protein p53
IL34	Interleukin 34	PC	Phosphatidylcholine
IL4I1	Interleukin-4-Induced Protein 1	PD-1	Programmed Cell Death Protein 1
IMC	Imaging Mass Cytometry	PDH	Pyruvate Dehydrogenase
Ki67	Antigen Ki-67, a Proliferation Marker	PE	Phosphatidylethanolamine
LDH	Lactate Dehydrogenase	PET	Positron Emission Tomography
LDHA	Lactate Dehydrogenase A	PGAM1	Phosphoglycerate Mutase 1
LLC	Lewis Lung Carcinoma	PGC1α	Peroxisome Proliferator-Activated Receptor γ Coactivator 1α
LOX	Lysyl Oxidase		
LUAD	Lung Adenocarcinoma		
M2	Alternatively Activated	pGluN2B	Phosphorylated GluN2B
MALDI-MSI	Matrix-Assisted Laser Desorption/ ionization Mass Spectrometry Imaging	PHGDH	Phosphoglycerate Dehydrogenase
		PPP	Pentose phosphate Pathway
MAPK	Mitogen-Activated Protein Kinase		

PPARγ	Peroxisome Proliferator-Activated Receptor γ
PRICKLE1	Prickle Planar Cell Polarity Protein 1
PTEN	Phosphatase and Tensin Homolog
PUFA; PUFAs	Polyunsaturated Fatty Acid; Polyunsaturated Fatty Acids
RAC2	Rac Family Small GTPase 2
RANO	Response Assessment in Neuro-Oncology
RARRES2	Retinoic Acid Receptor Responder 2 (gene encoding chemerin)
SEC61G	SEC61 Translocon Subunit Gamma
REDCAT	Raman Enhanced Delineation of Cell Atlases in Tissues
REST	RE1-Silencing Transcription Factor
RNA	Ribonucleic Acid
S1	Study-defined Tumor-surrounding Region Comprising Spatial Spots within about 105 μm of the Tumor Border
SCD1	Stearoyl-CoA Desaturase 1
SHP2	SH2 Domain-containing Protein Tyrosine Phosphatase 2
SIRPα	Signal Regulatory Protein α
SNMMI	Society of Nuclear Medicine and Molecular Imaging
Src	Proto-oncogene Tyrosine-protein Kinase Src
SREBP1	Sterol Regulatory Element-binding Protein 1
SUVmax	Maximum Standardized Uptake Value
T2-FLAIR	T2-Weighted Fluid-attenuated Inversion Recovery
TCA	Tricarboxylic Acid
TDO2	Tryptophan 2,3-Dioxygenase 2
TGFβ1	Transforming Growth Factor β1
TME	Tumor Microenvironment
TNBC	Triple-negative Breast Cancer
TRAP1	Tumor necrosis Factor Receptor-associated Protein 1
VEGFA	Vascular Endothelial Growth Factor A
VGF	VGF Nerve Growth Factor Inducible (neuropeptide precursor)
Wnt5a	Wnt Family Member 5A
xCT	Cystine-glutamate Antiporter
α-KG	α-Ketoglutarate
α-KGDH	α-Ketoglutarate Dehydrogenase

Author Contributions

Conceptualization, Methodology, Investigation, Writing—original draft: H.L.; Visualization, Writing—review & editing: H.L.; X.W.; Investigation, Supervision: Z.Z. All authors have read and agreed to the published version of the manuscript.

Conflicts of Interest

The authors declare no conflicts of interest.

Funding

The study did not receive any external funding and was conducted using only institutional resources.

Acknowledgments

The authors thank their home institutions (Division of Applied Oral Sciences & Community Dental Care, Faculty of Dentistry, The University of Hong Kong, Hong Kong SAR, China, and Department of Thoracic Surgery and Institute of Thoracic Oncology, West China Hospital, Sichuan University, Chengdu, China) for their general support.

AI Declaration

During manuscript preparation and revision, the authors used ChatGPT (models: GPT-5.6-sol and GPT-6-astra) and OpenAI Codex (desktop version 26.908) for language editing and organization. The authors critically reviewed and edited the outputs and remain responsible for the accuracy of the scientific claims and references. The authors take full responsibility for the accuracy, originality, integrity, and scientific content of the manuscript.

References

[1] Bhambhvani, H.P.; Granucci, M.; Rodrigues, A.; Kakusa, B.W.; Hayden Gephart, M. The Primary Sites Leading to Brain Metastases: Shifting Trends at a Tertiary Care Center. *J. Clin. Neurosci.* **2020**, *80*, 121–124. [CrossRef] [PubMed]

[2] Lu, Y.; Huang, Y.; Zhu, C.; Li, Z.; Zhang, B.; Sheng, H.; Li, H.; Liu, X.; Xu, Z.; Wen, Y.; et al. Cancer Brain Metastasis: Molecular Mechanisms and Therapeutic Strategies. *Mol. Biomed.* **2025**, *6*, 12. [CrossRef] [PubMed]

[3] Pinto, M.; Violante, S.; Cascão, R.; Faria, C.C. Unlocking the Role of Metabolic Pathways in Brain Metastatic Disease. *Cells* **2025**, *14*, 707. [CrossRef] [PubMed]

[4] Hsieh, W.-C.; Budiarto, B.R.; Wang, Y.-F.; Lin, C.-Y.; Gwo, M.-C.; So, D.K.; Tzeng, Y.-S.; Chen, S.-Y. Spatial Multi-Omics Analyses of the Tumor Immune Microenvironment. *J. Biomed. Sci.* **2022**, *29*, 96. [CrossRef] [PubMed]

[5] Karimi, E.; Yu, M.W.; Maritan, S.M.; Perus, L.J.M.; Rezanejad, M.; Sorin, M.; Dankner, M.; Fallah, P.; Doré, S.; Zuo, D.; et al. Single-Cell Spatial Immune Landscapes of Primary and Metastatic Brain

Tumours. *Nature* **2023**, *614*, 555–563. [CrossRef] [PubMed]

[6] Du, Y.; Ding, X.; Ye, Y. The Spatial Multi-Omics Revolution in Cancer Therapy: Precision Redefined. *Cell Rep. Med.* **2024**, *5*, 101740. [CrossRef] [PubMed]

[7] Kunachowicz, D.; Tomecka, P.; Sędzik, M.; Kalinin, J.; Kuźnicki, J.; Rembiałkowska, N. Influence of Hypoxia on Tumor Heterogeneity, DNA Repair, and Cancer Therapy: From Molecular Insights to Therapeutic Strategies. *Cells* **2025**, *14*, 1057. [CrossRef] [PubMed]

[8] Wu, C.; Xu, T.; Zhang, H.; Hu, Y.; Jiao, J.; Qiu, K.; Gu, J.; Li, W.; Sun, L. Hypoxia and Immunometabolism in the Tumor Microenvironment: Insights into Mechanisms and Therapeutic Potential. *Cancer Lett.* **2025**, *631*, 217913. [CrossRef] [PubMed]

[9] Parida, P.K.; Malladi, S. Metabolic Adaptations of Brain Metastasis. *Nat. Rev. Cancer* **2025**, *25*, 723–739. [CrossRef] [PubMed]

[10] Zhou, T.; Yan, Y.; Lin, M.; Zeng, C.; Mao, X.; Zhu, Y.; Han, J.; Li, D.-D.; Zhang, J. Astrocyte Involvement in Brain Metastasis: From Biological Mechanisms to Therapeutic Strategies. *Cancer Metastasis Rev.* **2025**, *44*, 60. [CrossRef] [PubMed]

[11] Zhang, Q.; Abdo, R.; Iosef, C.; Kaneko, T.; Cecchini, M.; Han, V.K.; Li, S.-C. The Spatial Transcriptomic Landscape of Non-Small Cell Lung Cancer Brain Metastasis. *Nat. Commun.* **2022**, *13*, 5983. [CrossRef] [PubMed]

[12] Biermann, J.; Melms, J.C.; Amin, A.D.; Wang, Y.; Caprio, L.A.; Karz, A.; Tagore, S.; Barrera, I.; Ibarra-Arellano, M.A.; Andreatta, M.; et al. Dissecting the Treatment-Naive Ecosystem of Human Melanoma Brain Metastasis. *Cell* **2022**, *185*, 2591–2608.e30. [CrossRef] [PubMed]

[13] Liu, K.; Wang, Y.; Wang, C.; Guo, C.; Zhang, D.; Zhong, Y.; Yin, L.; Lu, Y.; Liu, F.; Zhang, Y.; et al. Spatial Transcriptomics of Gastric Cancer Brain Metastasis Reveals Atypical Vasculature Strategies with Supportive Immune Profiles. *Gastroenterol. Rep.* **2024**, *12*, goae067. [CrossRef] [PubMed]

[14] Cheng, M.; Jiang, Y.; Xu, J.; Mentis, A.-F.A.; Wang, S.; Zheng, H.; Sahu, S.K.; Liu, L.; Xu, X. Spatially Resolved Transcriptomics: A Comprehensive Review of Their Technological Advances, Applications, and Challenges. *J. Genet. Genom.* **2023**, *50*, 625–640. [CrossRef] [PubMed]

[15] Marx, V. Method of the Year: Spatially Resolved Transcriptomics. *Nat. Methods* **2021**, *18*, 9–14. [CrossRef] [PubMed]

[16] Ozirmak Lermi, N.; Molina Ayala, M.; Hernandez, S.; Lu, W.; Khan, K.; Serrano, A.; Lubo, I.; Hamana, L.; Tomczak, K.; Barnes, S.; et al. Comparison of Imaging Based Single-Cell Resolution Spatial Transcriptomics Profiling Platforms Using Formalin-Fixed Paraffin-Embedded Tumor Samples. *Nat. Commun.* **2025**, *16*, 8499. [CrossRef] [PubMed]

[17] Sawant Dessai, A.; Kalhotra, P.; Novickis, A.T.; Dasgupta, S. Regulation of Tumor Metabolism by Post Translational Modifications on Metabolic Enzymes. *Cancer Gene Ther.* **2023**, *30*, 548–558. [CrossRef] [PubMed]

[18] Duncan, K.D.; Pětrošová, H.; Lum, J.J.; Goodlett, D.R. Mass Spectrometry Imaging Methods for Visualizing Tumor Heterogeneity. *Curr. Opin. Biotechnol.* **2024**, *86*, 103068. [CrossRef] [PubMed]

[19] Petrova, B.; Guler, A.T. Recent Developments in Single-Cell Metabolomics by Mass Spectrometry—A Perspective. *J. Proteome Res.* **2025**, *24*, 1493–1518. [CrossRef] [PubMed]

[20] Unsihuay, D.; Mesa Sanchez, D.; Laskin, J. Quantitative Mass Spectrometry Imaging of Biological Systems. *Annu. Rev. Phys. Chem.* **2021**, *72*, 307–329. [CrossRef] [PubMed]

[21] Wang, G.; van den Berg, B.M.; Kostidis, S.; Pinkham, K.; Jacobs, M.E.; Liesz, A.; Giera, M.; Rabelink, T.J. Spatial Quantitative Metabolomics Enables Identification of Remote and Sustained Ipsilateral Cortical Metabolic Reprogramming After Stroke. *Nat. Metab.* **2025**, *7*, 1791–1800. [CrossRef] [PubMed]

[22] Samarah, L.Z.; Zheng, C.; Xing, X.; Lee, W.D.; Afriat, A.; Chitra, U.; MacArthur, M.R.; Lu, W.; Jankowski, C.S.R.; Ma, C.; et al. Spatial Metabolic Gradients in the Liver and Small Intestine. *Nature* **2025**, *648*, 182–190. [CrossRef] [PubMed]

[23] Tian, R.; Xue, Z.; Chen, Y.; Qi, Y.; Zhang, J.; Yuan, J.; Ruan, D.; Lin, J.; Liu, J.; Wang, D.; et al. Integrating Cross-Sample and Cross-Modal Data for Spatial Transcriptomics and Metabolomics with SpatialMETA. *Nat. Commun.* **2025**, *16*, 8855. [CrossRef] [PubMed]

[24] Liu, X.; Peng, T.; Xu, M.; Lin, S.; Hu, B.; Chu, T.; Liu, B.; Xu, Y.; Ding, W.; Li, L.; et al. Spatial Multi-Omics: Deciphering Technological Landscape of Integration of Multi-Omics and Its Applications. *J. Hematol. Oncol.* **2024**, *17*, 72. [CrossRef] [PubMed]

[25] Wess, M.; Andersen, M.K.; Midtbust, E.; Guillem, J.C.C.; Viset, T.; Størkersen, Ø.; Krossa, S.; Rye, M.B.; Tessem, M.-B. Spatial Integration of Multi-Omics Data from Serial Sections Using the Novel Multi-Omics Imaging Integration Toolset. *GigaScience* **2025**, *14*, giaf035. [CrossRef] [PubMed]

[26] Kim, D.Y.; Lee, J.; Choi, J.; Shin, H.; Lee, J.S.; Kim, E.J. Spatial Multi-Omics in Precision Medicine: Integrating Biological Insights Through Multidisciplinary Collaboration. *Semin. Cancer Biol.* **2026**, *119*, 24–37. [CrossRef] [PubMed]

[27] Vicari, M.; Mirzazadeh, R.; Nilsson, A.; Shariatgorji, R.; Bjärterot, P.; Larsson, L.; Lee, H.; Nilsson, M.; Foyer, J.; Ekvall, M.; et al. Spatial Multimodal Analysis of Transcriptomes and Metabolomes in Tissues. *Nat. Biotechnol.* **2024**, *42*, 1046–1050. [CrossRef] [PubMed]

[28] Li, Y.; Zhang, Z.; Enninful, A.; Farzad, N.; Rajbhandari, P.; Tian, H.; Nam, J.; Qin, X.; Villazon, J.; Fung, A.A.; et al. All-Optical Multimodal Map-

ping of Single-Cell-Type-Specific Metabolic Activities via REDCAT. *Nat. Methods* **2026**, *23*, 1840–1853. [CrossRef] [PubMed]

[29] Tobar, L.E.; Farnsworth, R.H.; Stacker, S.A. Brain Vascular Microenvironments in Cancer Metastasis. *Biomolecules* **2022**, *12*, 401. [CrossRef] [PubMed]

[30] Lockman, P.R.; Mittapalli, R.K.; Taskar, K.S.; Rudraraju, V.; Gril, B.; Bohn, K.A.; Adkins, C.E.; Roberts, A.; Thorsheim, H.R.; Gaasch, J.A.; et al. Heterogeneous Blood–Tumor Barrier Permeability Determines Drug Efficacy in Experimental Brain Metastases of Breast Cancer. *Clin. Cancer Res.* **2010**, *16*, 5664–5678. [CrossRef] [PubMed]

[31] Bång-Rudenstam, A.; Cerezo-Magaña, M.; Horvath, M.; Talbot, H.; Gustafsson, E.; Jonathan, S.; Chakraborty, C.; Nissen, I.; Gonçalves de Oliveira, K.; Boukredine, A.; et al. Tumour Acidosis Remodels the Glycocalyx to Control Lipid Scavenging and Ferroptosis. *Nat. Cell Biol.* **2026**, *28*, 567–580. [CrossRef] [PubMed]

[32] Berghoff, A.S.; Rajky, O.; Winkler, F.; Bartsch, R.; Furtner, J.; Hainfellner, J.A.; Goodman, S.L.; Weller, M.; Schittenhelm, J.; Preusser, M. Invasion Patterns in Brain Metastases of Solid Cancers. *Neuro-Oncology* **2013**, *15*, 1664–1672. [CrossRef] [PubMed]

[33] Garzia, L. Astrocytes Are Enablers of Brain Metastases. *Nat. Cell Biol.* **2024**, *26*, 1632–1633. [CrossRef] [PubMed]

[34] Chen, P.; Zuo, Y.; Wang, M.; Liu, R.; Li, Y.; Wang, Z.; Huang, H.; Luo, X.; Wang, W.; Wu, Y.; et al. Lung Cancer Cells Upregulate Stearoyl-CoA Desaturase 1 in Microglia by Activating the STAT3 Pathway to Change Microglial Inflammatory Response in Lung-to-Brain Metastases. *Cell Death Dis.* **2025**, *16*, 702. [CrossRef] [PubMed]

[35] Maritan, S.M.; Karimi, E.; Dankner, M.; Hernandez-Corchado, A.; Yu, M.W.; Annis, M.G.; Aghazadeh Habashi, Y.; Rezanejad, M.; Liu, B.; Koudieh, N.; et al. Distinct Immune Landscapes Characterize Highly Versus Minimally Invasive Brain Metastases. *JCI Insight* **2026**, *11*, e199498. [CrossRef] [PubMed]

[36] Zeng, Q.; Michael, I.P.; Zhang, P.; Saghafinia, S.; Knott, G.; Jiao, W.; McCabe, B.D.; Galván, J.A.; Robinson, H.P.C.; Zlobec, I.; et al. Synaptic Proximity Enables NMDAR Signalling to Promote Brain Metastasis. *Nature* **2019**, *573*, 526–531. [CrossRef] [PubMed]

[37] Yoo, J.; Park, I.; Kim, H.J.; Park, H.H.; Lee, S.; Kim, J.H.; Cha, Y.J. Spatial Transcriptomic Landscape of Brain Metastases from Triple-Negative Breast Cancer: Comparison of Primary Tumor and Brain Metastases Using Spatial Analysis. *Cancer Res. Treat.* **2026**, *58*, 182–197. [CrossRef] [PubMed]

[38] Tsyben, A.; Dannhorn, A.; Hamm, G.; Pitoulias, M.; Couturier, D.-L.; Sawle, A.; Briggs, M.; Wright, A.J.; Brodie, C.; Mendil, L.; et al. Cell-Intrinsic Metabolic Phenotypes Identified in Patients with Glioblastoma, Using Mass Spectrometry Imaging of ^{13}C-Labelled Glucose Metabolism. *Nat. Metab.* **2025**, *7*, 928–939. [CrossRef] [PubMed]

[39] Palmieri, D.; Fitzgerald, D.; Shreeve, S.M.; Hua, E.; Bronder, J.L.; Weil, R.J.; Davis, S.; Stark, A.M.; Merino, M.J.; Kurek, R.; et al. Analyses of Resected Human Brain Metastases of Breast Cancer Reveal the Association Between Up-Regulation of Hexokinase 2 and Poor Prognosis. *Mol. Cancer Res.* **2009**, *7*, 1438–1445. [CrossRef] [PubMed]

[40] Zhou, C.; Yang, Y.; Cui, H.; Li, S.; Wang, Z.; Chen, L.; Feng, M.; Li, D.; Chen, X.; Hao, B.; et al. SEC61G Facilitates Brain Metastases via Antagonizing PGAM1 Ubiquitination and Immune Microenvironment Remodeling in Non-Small Cell Lung Cancer. *Int. J. Biol. Sci.* **2025**, *21*, 1436–1458. [CrossRef] [PubMed]

[41] Dong, T.; Liu, Z.; Xuan, Q.; Wang, Z.; Ma, W.; Zhang, Q. Tumor LDH-A Expression and Serum LDH Status Are Two Metabolic Predictors for Triple Negative Breast Cancer Brain Metastasis. *Sci. Rep.* **2017**, *7*, 6069. [CrossRef] [PubMed]

[42] Liu, S.; Bai, Z.; Qiao, Y.; Ge, Y.; Qu, F.; Li, M.; Wang, J.; Shi, X.; Ma, Y.; Li, J.; et al. Lactate Dehydrogenase A–Mediated CREB1 Lactylation Promotes Breast Cancer Brain Metastasis by Transcriptionally Activating Cytoskeletal Remodeling. *Neuro Oncol.* **2026**, *28*, 1970–1985. [CrossRef] [PubMed]

[43] Yi, Y.; Xu, W.; Yu, H.; Luo, Y.; Zeng, F.; Luo, D.; Zeng, Z.; Xiong, L.; Huang, L.; Cai, J.; et al. Integrated Multi-Omics Reveals Glycolytic Gene Signatures of Lung Adenocarcinoma Brain Metastasis and the Impact of Rac2 Lactylation on Immunosuppressive Microenvironment. *J. Transl. Med.* **2025**, *23*, 1193. [CrossRef] [PubMed]

[44] Cha, Y.J.; Jung, W.H.; Koo, J.S. Differential Site-Based Expression of Pentose Phosphate Pathway-Related Proteins Among Breast Cancer Metastases. *Dis. Markers* **2017**, *2017*, 7062517. [CrossRef] [PubMed]

[45] Chen, E.I.; Hewel, J.; Krueger, J.S.; Tiraby, C.; Weber, M.R.; Kralli, A.; Becker, K.; Yates, J.R., III; Felding-Habermann, B. Adaptation of Energy Metabolism in Breast Cancer Brain Metastases. *Cancer Res.* **2007**, *67*, 1472–1486. [CrossRef] [PubMed]

[46] Mashimo, T.; Pichumani, K.; Vemireddy, V.; Hatanpaa, K.J.; Singh, D.K.; Sirasanagandla, S.; Nannepaga, S.; Piccirillo, S.G.; Kovacs, Z.; Foong, C.; et al. Acetate Is a Bioenergetic Substrate for Human Glioblastoma and Brain Metastases. *Cell* **2014**, *159*, 1603–1614. [CrossRef] [PubMed]

[47] Esquea, E.M.; Ciraku, L.; Young, R.G.; Merzy, J.; Talarico, A.N.; Ahmed, N.N.; Karuppiah, M.; Ramesh, A.; Chatoff, A.; Crispim, C.V.; et al. Selective and Brain-Penetrant ACSS2 Inhibitors Target Breast Cancer Brain Metastatic Cells. *Front. Pharmacol.* **2024**, *15*, 1394685. [CrossRef] [PubMed]

[48] Young, R.G.; Esquea, E.M.; Ciraku, L.; Merzy, J.; Ahmed, N.N.; Talarico, A.N.; Karuppiah, M.; Medori, S.M.; Warade, R.P.; Gocal, W.; et al. ACSS2 Suppresses Ferroptosis to Drive Breast Cancer Brain

Metastasis. *Cancer Res.* **2026**, *86*, 3502–3518. [CrossRef] [PubMed]

[49] Ngo, B.; Kim, E.; Osorio-Vasquez, V.; Doll, S.; Bustraan, S.; Liang, R.J.; Luengo, A.; Davidson, S.M.; Ali, A.; Ferraro, G.B.; et al. Limited Environmental Serine and Glycine Confer Brain Metastasis Sensitivity to PHGDH Inhibition. *Cancer Discov.* **2020**, *10*, 1352–1373. [CrossRef] [PubMed]

[50] Mao, L.; Wang, L.; Lyu, Y.; Zhuang, Q.; Li, Z.; Zhang, J.; Gu, Z.; Lu, S.; Wang, X.; Guan, Y.; et al. Branch Chain Amino Acid Metabolism Promotes Brain Metastasis of NSCLC Through EMT Occurrence by Regulating ALKBH5 Activity. *Int. J. Biol. Sci.* **2024**, *20*, 3285–3301. [CrossRef] [PubMed]

[51] Wu, Y.; Derks, S.H.A.E.; Wood, T.C.; de Blois, E.; van der Veldt, A.A.M.; Smits, M.; Warnert, E.A.H. Improved Postprocessing of Dynamic Glucose-Enhanced CEST MRI for Imaging Brain Metastases at 3 T. *Eur. Radiol. Exp.* **2023**, *7*, 78. [CrossRef] [PubMed]

[52] Cappelletto, N.I.C.; Soliman, H.; Uthayakumar, B.; Sahgal, A.; Bragagnolo, N.D.; Chen, A.P.; Endre, R.; Ma, N.; Perks, W.J.; Detsky, J.S.; et al. Hyperpolarized ^{13}C Lactate-to-Bicarbonate Signal Ratio Predicts Brain Metastases Response to Stereotactic Radiosurgery. *Neurooncol. Adv.* **2025**, *7*, vdaf121. [CrossRef] [PubMed]

[53] Cappelletto, N.I.C.; Soliman, H.; Uthayakumar, B.; Sahgal, A.; Chen, A.P.; Endre, R.; Ma, N.; Perks, W.J.; Detsky, J.S.; Heyn, C.; et al. Widespread Elevated Hyperpolarized ^{13}C-Lactate and ^{13}C-Bicarbonate Signal in the Brain of Patients with Brain Metastases Undergoing Treatment. *Sci. Rep.* **2026**. [CrossRef]

[54] Tang, J.; Zhao, Y.; Chen, L.; Liu, Y.; Xie, H.; Wu, Z.; Zhang, L.; Fan, D.; Xu, X.; Ai, L.; et al. Distribution of Glutamate and Glutamine in Tumor Microenvironments of Brain Metastasis: Insights from Biochemical Analysis and Molecular Imaging. *iScience* **2025**, *28*, 113371. [CrossRef] [PubMed]

[55] Ishibashi, K.; Ichinose, T.; Kadokawa, R.; Mizutani, R.; Iwabuchi, S.; Togi, S.; Ura, H.; Tange, S.; Shinjo, K.; Nakayama, J.; et al. Astrocyte-Induced mGluR1 Activates Human Lung Cancer Brain Metastasis via Glutamate-Dependent Stabilization of EGFR. *Dev. Cell* **2024**, *59*, 579–594.e6. [CrossRef] [PubMed]

[56] Ruan, X.; Yan, W.; Cao, M.; Daza, R.A.M.; Fong, M.Y.; Yang, K.; Wu, J.; Liu, X.; Palomares, M.; Wu, X.; et al. Breast Cancer Cell-Secreted miR-199b-5p Hijacks Neurometabolic Coupling to Promote Brain Metastasis. *Nat. Commun.* **2024**, *15*, 4549. [CrossRef] [PubMed]

[57] Di Russo, S.; Borsatti, G.E.; Bouzidi, A.; Liberati, F.R.; Riva, A.; Tripodi, F.; Rolfi, L.R.; Spizzichino, S.; Tramutola, A.; Perluigi, M.; et al. NF-κB-Mediated Cytokine Secretion and Glutamate Metabolic Reprogramming Converge in Breast Cancer Brain Tropism. *Cancer Lett.* **2025**, *630*, 217907. [CrossRef] [PubMed]

[58] Parida, P.K.; Marquez-Palencia, M.; Nair, V.; Kaushik, A.K.; Kim, K.; Sudderth, J.; Quesada-Diaz, E.; Cajigas, A.; Vemireddy, V.; Gonzalez-Ericsson, P.I.; et al. Metabolic Diversity Within Breast Cancer Brain-Tropic Cells Determines Metastatic Fitness. *Cell Metab.* **2022**, *34*, 90–105.e7. [CrossRef] [PubMed]

[59] Schnepp, P.M.; Lee, D.D.; Guldner, I.H.; O'Tighearnaigh, T.K.; Howe, E.N.; Palakurthi, B.; Eckert, K.E.; Toni, T.A.; Ashfeld, B.L.; Zhang, S. GAD1 Upregulation Programs Aggressive Features of Cancer Cell Metabolism in the Brain Metastatic Microenvironment. *Cancer Res.* **2017**, *77*, 2844–2856. [CrossRef] [PubMed]

[60] Xie, M.; Qin, H.; Liu, L.; Wu, J.; Zhao, Z.; Zhao, Y.; Fang, Y.; Yu, X.; Su, C. GABA Regulates Metabolic Reprogramming to Mediate the Development of Brain Metastasis in Non-Small Cell Lung Cancer. *J. Exp. Clin. Cancer Res.* **2025**, *44*, 61. [CrossRef] [PubMed]

[61] Wu, S.-Y.; Tyagi, A.; Smith, E.C.; Lee, J.S.; Perng, P.S.; Kuo, Y.-M.; Wang, T.-F.; Chen, H.-F.; Deshpande, R.P.; Kim, J.W.; et al. GABA Shunt Metabolism Drives Smoking-Related Peri-Neuronal Brain Metastasis by Hijacking Synaptic Signaling. *Neuro Oncol.* **2026**, noag201. [CrossRef] [PubMed]

[62] Tyagi, A.; Wu, S.Y.; Watabe, K. Metabolism in the Progression and Metastasis of Brain Tumors. *Cancer Lett.* **2022**, *539*, 215713. [CrossRef] [PubMed]

[63] Ferraro, G.B.; Ali, A.; Luengo, A.; Kodack, D.P.; Deik, A.; Abbott, K.L.; Bezwada, D.; Blanc, L.; Prideaux, B.; Jin, X.; et al. Fatty Acid Synthesis Is Required for Breast Cancer Brain Metastasis. *Nat. Cancer* **2021**, *2*, 414–428. [CrossRef] [PubMed]

[64] Cordero, A.; Kanojia, D.; Miska, J.; Panek, W.K.; Xiao, A.; Han, Y.; Bonamici, N.; Zhou, W.; Xiao, T.; Wu, M.; et al. FABP7 Is a Key Metabolic Regulator in HER2+ Breast Cancer Brain Metastasis. *Oncogene* **2019**, *38*, 6445–6460. [CrossRef] [PubMed]

[65] Li, J.; Ouyang, S.; Lin, Z.; Peng, K.; Yan, J.; Lu, M.; Ding, W.; Mo, J.; Su, Y.; Wang, L.; et al. The IGF2BP3–FASN Axis Drives Lipid Metabolic Reprogramming to Promote Brain Colonization in Non-Small Cell Lung Cancer. *Cell Death Dis.* **2025**, *16*, 684. [CrossRef] [PubMed]

[66] Li, Y.-Q.; Sun, F.-Z.; Li, C.-X.; Mo, H.-N.; Zhou, Y.-T.; Lv, D.; Zhai, J.-T.; Qian, H.-L.; Ma, F. RARRES2 Regulates Lipid Metabolic Reprogramming to Mediate the Development of Brain Metastasis in Triple Negative Breast Cancer. *Mil. Med. Res.* **2023**, *10*, 34. [CrossRef] [PubMed]

[67] Roux, A.; Winnard, P.T., Jr.; Van Voss, M.H.; Muller, L.; Jackson, S.N.; Hoffer, B.; Woods, A.S.; Raman, V. MALDI-MSI of Lipids in a Model of Breast Cancer Brain Metastasis Provides a Surrogate Measure of Ischemia/Hypoxia. *Mol. Cell. Biochem.* **2023**, *478*, 2567–2580. [CrossRef] [PubMed]

[68] Chen, B.; Kiang, K.M.; Liu, F.; Li, C.; Li, X.; Weiwei, C.; Fu, X.; Xiao, G.; Sun, J.; Da, E.; et al. Neutrophil Extracellular Trap Reprograms Cancer

Metabolism to Form a Metastatic Niche Promoting Non-Small Cell Lung Cancer Brain Metastasis. *Adv. Sci.* **2026**, *13*, e08478. [CrossRef] [PubMed]

[69] Yang, Y.; Gao, Y.; Qi, Z.; Li, S.; Wang, Z.; Li, D.; Chen, L.; Zhou, C.; Feng, M.; Chen, X.; et al. Single-Cell and Spatial Transcriptomes Reveal Oligodendrocyte Remodeling Fatty Acid Metabolism Microenvironment of Lung Cancer Brain Metastases. *J. Transl. Med.* **2026**, *24*, 1099. [CrossRef] [PubMed]

[70] Laue, K.; Pozzi, S.; Zerbib, J.; Bertolio, R.; Eliezer, Y.; Cohen-Sharir, Y.; Winkler, T.; Caputo, M.; Ricci, A.A.; Adler, L.; et al. p53 Inactivation Drives Breast Cancer Metastasis to the Brain Through SCD1 Upregulation and Increased Fatty Acid Metabolism. *Nat. Genet.* **2026**, *58*, 116–131. [CrossRef] [PubMed]

[71] Zou, Y.; Watters, A.; Cheng, N.; Perry, C.E.; Xu, K.; Alicea, G.M.; Parris, J.L.D.; Baraban, E.; Ray, P.; Nayak, A.; et al. Polyunsaturated Fatty Acids from Astrocytes Activate PPARγ Signaling in Cancer Cells to Promote Brain Metastasis. *Cancer Discov.* **2019**, *9*, 1720–1735. [CrossRef] [PubMed]

[72] Greene, J.; Segaran, A.; Lord, S. Targeting OXPHOS and the Electron Transport Chain in Cancer; Molecular and Therapeutic Implications. *Semin. Cancer Biol.* **2022**, *86*, 851–859. [CrossRef] [PubMed]

[73] Porporato, P.E.; Filigheddu, N.; Bravo-San Pedro, J.M.; Kroemer, G.; Galluzzi, L. Mitochondrial Metabolism and Cancer. *Cell Res.* **2018**, *28*, 265–280. [CrossRef] [PubMed]

[74] Yang, Z.; Wei, S.; Duan, H.; Wang, X.; Zhang, D.; Kiang, K.M.-Y.; Deng, Y.; Yang, Y.; Ku, Y.; Hu, W.; et al. A Proteogenomic Atlas of 1032 Brain Metastases Identifies Molecular Subtypes, Immune Landscapes, and Therapeutic Vulnerabilities. *Nat. Commun.* **2026**, *17*, 2038. [CrossRef] [PubMed]

[75] Guedes, J.; Woldmar, N.; Baltas, E.; Kriston, A.; Migh, E.; Kovács, F.; Oskolás, H.; Marko-Varga, M.; Appelqvist, R.; Wieslander, E.; et al. AI-Based Digital Pathology and Spatial Proteomics Enable Precision Oncology: A Case Report of Recurrent Melanoma in a Young Patient. *npj Precis. Oncol.* **2026**, *10*, 296. [CrossRef] [PubMed]

[76] Fantin, J.; Toutain, J.; Pérès, E.A.; Bernay, B.; Mehani, S.M.; Helaine, C.; Bourgeois, M.; Brunaud, C.; Chazalviel, L.; Pontin, J.; et al. Assessment of Hypoxia and Oxidative-Related Changes in a Lung-Derived Brain Metastasis Model by [^{64}Cu][Cu(ATSM)] PET and Proteomic Studies. *EJNMMI Res.* **2023**, *13*, 102. [CrossRef] [PubMed]

[77] Corroyer-Dulmont, A.; Valable, S.; Fantin, J.; Chatre, L.; Toutain, J.; Teulier, S.; Bazille, C.; Letissier, E.; Levallet, J.; Divoux, D.; et al. Multimodal Evaluation of Hypoxia in Brain Metastases of Lung Cancer and Interest of Hypoxia Image-Guided Radiotherapy. *Sci. Rep.* **2021**, *11*, 11239. [CrossRef] [PubMed]

[78] Alvaro-Espinosa, L.; Marquez-Galera, A.; Priego, N.; García-Calvo, V.; Perea-García, M.; Hernandez-Oliver, C.; Retana, D.; Sanchez, O.; de Pablos-Aragoneses, A.; García-Gómez, P.; et al. MIF-Induced CD74+ Microglia and Macrophages Promote Progression of Brain Metastasis and Are Clinically Relevant Across Central Nervous System Disorders. *Cancer Res.* **2026**, *86*, 3249–3269. [CrossRef] [PubMed]

[79] Tsai, Y.-T.; Mackert, J.D.; Wilson, A.; Kooshki, M.; Payne, V.; Sagastume, J.J.; Szymonski, A.; Westwood, B.; Miller, L.D.; Triozzi, P.L.; et al. Cancer-Intrinsic SIRPα Signaling Triggers Mitochondrial Fission and Immune Tolerance to Promote TNBC Breast-to-Brain Metastasis. *Neuro Oncol.* **2026**, noag202. [CrossRef] [PubMed]

[80] Wang, Y.; Sheng, X.; Yang, Y.; Liu, C.; Wang, S.; Guo, R.; Gu, Y.; Chen, M.; Zhang, H.; Du, J.; et al. VGF-Mediated Mitochondrial Remodeling Fuels Lung Adenocarcinoma Brain Metastasis. *Cancer Res.* **2026**, *86*, 2104–2125. [CrossRef] [PubMed]

[81] Lin, M.; Wen, Z.; Zeng, C.; Jin, Y.; Zhou, T.; Yan, Y.; Huang, S.; Hu, X.; Guan, X.; Hu, X.; et al. Complex I Protein NDUFB9 Is a Metabolic Vulnerability in Triple Negative Breast Cancer Brain Metastases. *Nat. Commun.* **2026**, *17*, 6262. [CrossRef] [PubMed]

[82] Fukumura, K.; Malgulwar, P.B.; Fischer, G.M.; Hu, X.; Mao, X.; Song, X.; Hernandez, S.D.; Zhang, X.H.; Zhang, J.; Parra, E.R.; et al. Multi-Omic Molecular Profiling Reveals Potentially Targetable Abnormalities Shared Across Multiple Histologies of Brain Metastasis. *Acta Neuropathol.* **2021**, *141*, 303–321. [CrossRef] [PubMed]

[83] Xiao, L.; Zhou, J.; Liu, H.; Zhou, Y.; Chen, W.; Cui, W.; Zhao, Y. RNA Sequence Profiling Reveals Unique Immune and Metabolic Features of Breast Cancer Brain Metastases. *Front. Oncol.* **2021**, *11*, 679262. [CrossRef] [PubMed]

[84] Xiao, Y.; Hu, F.; Chi, Q. Single-Cell RNA Sequencing and Spatial Transcriptome Reveal Potential Molecular Mechanisms of Lung Cancer Brain Metastasis. *Int. Immunopharmacol.* **2024**, *140*, 112804. [CrossRef] [PubMed]

[85] Xing, X.; Zhong, J.; Biermann, J.; Duan, H.; Zhang, X.; Shi, Y.; Gao, Y.; He, K.; Zhai, D.; Luo, F.; et al. Pan-Cancer Human Brain Metastases Atlas at Single-Cell Resolution. *Cancer Cell* **2025**, *43*, 1242–1260.e9. [CrossRef] [PubMed]

[86] Fischer, G.M.; Guerrieri, R.A.; Hu, Q.; Joon, A.Y.; Kumar, S.; Haydu, L.E.; McQuade, J.L.; Vashisht Gopal, Y.N.; Knighton, B.; Deng, W.; et al. Clinical, Molecular, Metabolic, and Immune Features Associated with Oxidative Phosphorylation in Melanoma Brain Metastases. *Neurooncol. Adv.* **2021**, *3*, vdaa177. [CrossRef] [PubMed]

[87] Guerrieri, R.A.; Fischer, G.M.; Kircher, D.A.; Joon, A.Y.; Cortez, J.R.; Grossman, A.H.; Hudgens, C.W.; Ledesma, D.A.; Lazcano, R.; Onana, C.Y.; et al. Oxidative Phosphorylation (OXPHOS) Promotes the Formation and Growth of Melanoma Lung and Brain Metastases. *bioRxiv* **2025**. [CrossRef] [PubMed]

[88] Duan, H.; Ren, J.; Wei, S.; Yang, Z.; Li, C.; Wang, Z.; Li, M.; Wei, Z.; Liu, Y.; Wang, X.; et al. Integrated Analyses of Multi-Omic Data Derived from Paired Primary Lung Cancer and Brain Metastasis Reveal

the Metabolic Vulnerability as a Novel Therapeutic Target. *Genome Med.* **2024**, *16*, 138. [CrossRef] [PubMed]

[89] Burns, T.F.; Dacic, S.; Chakka, A.; Miller, E.; Velez, M.A.; Somasundaram, A.; Bhattacharya, S.; Gaither-Davis, A.; Devadassan, P.; Jin, J.; et al. MET Alterations Are Enriched in Lung Adenocarcinoma Brain Metastases, Defining a Distinct Biologic Subtype. *J. Clin. Invest.* **2026**, *136*, e194708. [CrossRef] [PubMed]

[90] Harding, J.J.; Telli, M.; Munster, P.; Voss, M.H.; Infante, J.R.; DeMichele, A.; Dunphy, M.; Le, M.H.; Molineaux, C.; Orford, K.; et al. A Phase I Dose-Escalation and Expansion Study of Telaglenastat in Patients with Advanced or Metastatic Solid Tumors. *Clin. Cancer Res.* **2021**, *27*, 4994–5003. [CrossRef] [PubMed]

[91] Gouda, M.A.; Voss, M.H.; Tawbi, H.; Gordon, M.; Tykodi, S.S.; Lam, E.T.; Vaishampayan, U.; Tannir, N.M.; Chaves, J.; Nikolinakos, P.; et al. A Phase I/II Study of the Safety and Efficacy of Telaglenastat (CB-839) in Combination with Nivolumab in Patients with Metastatic Melanoma, Renal Cell Carcinoma, and Non-Small-Cell Lung Cancer. *ESMO Open* **2025**, *10*, 104536. [CrossRef] [PubMed]

[92] Serhan, H.A.; Bao, L.; Cheng, X.; Qin, Z.; Liu, C.-J.; Heth, J.A.; Udager, A.M.; Soellner, M.B.; Merajver, S.D.; Morikawa, A.; et al. Targeting Fatty Acid Synthase in Preclinical Models of TNBC Brain Metastases Synergizes with SN-38 and Impairs Invasion. *npj Breast Cancer* **2024**, *10*, 43. [CrossRef] [PubMed]

[93] Fischer, G.M.; Jalali, A.; Kircher, D.A.; Lee, W.-C.; McQuade, J.L.; Haydu, L.E.; Joon, A.Y.; Reuben, A.; de Macedo, M.P.; Carapeto, F.C.L.; et al. Molecular Profiling Reveals Unique Immune and Metabolic Features of Melanoma Brain Metastases. *Cancer Discov.* **2019**, *9*, 628–645. [CrossRef] [PubMed]

[94] Yap, T.A.; Daver, N.; Mahendra, M.; Zhang, J.; Kamiya-Matsuoka, C.; Meric-Bernstam, F.; Kantarjian, H.M.; Ravandi, F.; Collins, M.E.; Francesco, M.E.D.; et al. Complex I Inhibitor of Oxidative Phosphorylation in Advanced Solid Tumors and Acute Myeloid Leukemia: Phase I Trials. *Nat. Med.* **2023**, *29*, 115–126. [CrossRef] [PubMed]

[95] Parida, P.K.; Marquez-Palencia, M.; Ghosh, S.; Khandelwal, N.; Kim, K.; Nair, V.; Liu, X.-Z.; Vu, H.S.; Zacharias, L.G.; Gonzalez-Ericsson, P.I.; et al. Limiting Mitochondrial Plasticity by Targeting DRP1 Induces Metabolic Reprogramming and Reduces Breast Cancer Brain Metastases. *Nat. Cancer* **2023**, *4*, 893–907. [CrossRef] [PubMed]

[96] Bordt, E.A.; Clerc, P.; Roelofs, B.A.; Saladino, A.J.; Tretter, L.; Adam-Vizi, V.; Cherok, E.; Khalil, A.; Yadava, N.; Ge, S.X.; et al. The Putative Drp1 Inhibitor mdivi-1 Is a Reversible Mitochondrial Complex I Inhibitor That Modulates Reactive Oxygen Species. *Dev. Cell* **2017**, *40*, 583–594.e6. [CrossRef] [PubMed]

[97] Marullo, R.; Castro, M.; Yomtoubian, S.; Calvo-Vidal, M.N.; Revuelta, M.V.; Krumsiek, J.; Cho, A.; Morgado, P.C.; Yang, S.; Medina, V.; et al. The Metabolic Adaptation Evoked by Arginine Enhances the Effect of Radiation in Brain Metastases. *Sci. Adv.* **2021**, *7*, eabg1964. [CrossRef] [PubMed]

[98] Liu, X.; Du, G.; Mu, N.; He, L. A Pharmacodynamic Study of Rapid Lactate Metabolic Modulation by Intravenous L-Arginine in Brain Metastases. *Front. Oncol.* **2026**, *16*, 1845249. [CrossRef] [PubMed]

[99] Evangeliou, A.E.; Spilioti, M.G.; Vassilakou, D.; Goutsaridou, F.; Seyfried, T.N. Restricted Ketogenic Diet Therapy for Primary Lung Cancer with Metastasis to the Brain: A Case Report. *Cureus* **2022**, *14*, e27603. [CrossRef] [PubMed]

[100] Takada, T.; Takata, K.; Ashihara, E. Inhibition of Monocarboxylate Transporter 1 Suppresses the Proliferation of Glioblastoma Stem Cells. *J. Physiol. Sci.* **2016**, *66*, 387–396. [CrossRef] [PubMed]

[101] Hanaford, A.R.; Alt, J.; Rais, R.; Wang, S.Z.; Kaur, H.; Thorek, D.L.J.; Eberhart, C.G.; Slusher, B.S.; Martin, A.M.; Raabe, E.H. Orally Bioavailable Glutamine Antagonist Prodrug JHU-083 Penetrates Mouse Brain and Suppresses the Growth of MYC-Driven Medulloblastoma. *Transl. Oncol.* **2019**, *12*, 1314–1322. [CrossRef] [PubMed]

[102] Yamashita, A.S.; da Costa Rosa, M.; Stumpo, V.; Rais, R.; Slusher, B.S.; Riggins, G.J. The Glutamine Antagonist Prodrug JHU-083 Slows Malignant Glioma Growth and Disrupts mTOR Signaling. *Neuro-Oncol. Adv.* **2021**, *3*, vdaa149. [CrossRef] [PubMed]

[103] Leone, R.D.; Zhao, L.; Englert, J.M.; Sun, I.-M.; Oh, M.-H.; Sun, I.-H.; Arwood, M.L.; Bettencourt, I.A.; Patel, C.H.; Wen, J.; et al. Glutamine Blockade Induces Divergent Metabolic Programs to Overcome Tumor Immune Evasion. *Science* **2019**, *366*, 1013–1021. [CrossRef] [PubMed]

[104] Lin, H.; Patel, S.; Affleck, V.S.; Wilson, I.; Turnbull, D.M.; Joshi, A.R.; Maxwell, R.; Stoll, E.A. Fatty Acid Oxidation Is Required for the Respiration and Proliferation of Malignant Glioma Cells. *Neuro-Oncology* **2017**, *19*, 43–54. [CrossRef] [PubMed]

[105] Shim, J.-K.; Choi, S.; Yoon, S.-J.; Choi, R.J.; Park, J.; Lee, E.H.; Cho, H.J.; Lee, S.; Teo, W.-Y.; Moon, J.H.; et al. Etomoxir, a Carnitine Palmitoyltransferase 1 Inhibitor, Combined with Temozolomide Reduces Stemness and Invasiveness in Patient-Derived Glioblastoma Tumorspheres. *Cancer Cell Int.* **2022**, *22*, 309. [CrossRef] [PubMed]

[106] Divakaruni, A.S.; Hsieh, W.Y.; Minarrieta, L.; Duong, T.N.; Kim, K.K.O.; Desousa, B.R.; Andreyev, A.Y.; Bowman, C.E.; Caradonna, K.; Dranka, B.P.; et al. Etomoxir Inhibits Macrophage Polarization by Disrupting CoA Homeostasis. *Cell Metab.* **2018**, *28*, 490–503.e7. [CrossRef] [PubMed]

[107] Guardado Rivas, M.O.; Stuart, S.D.; Thach, D.; Dahan, M.; Shorr, R.; Zachar, Z.; Bingham, P.M. Evidence for a Novel, Effective Approach to Targeting Carcinoma Catabolism Exploiting the First-in-Class,

Anti-Cancer Mitochondrial Drug, CPI-613. *PLoS ONE* **2022**, *17*, e0269620. [CrossRef] [PubMed]

[108] Philip, P.A.; Sahai, V.; Bahary, N.; Mahipal, A.; Kasi, A.; Rocha Lima, C.M.S.; Alistar, A.T.; Oberstein, P.E.; Golan, T.; Metges, J.-P.; et al. Devimistat (CPI-613) With Modified Fluorouarcil, Oxaliplatin, Irinotecan, and Leucovorin (FFX) Versus FFX for Patients With Metastatic Adenocarcinoma of the Pancreas: The Phase III AVENGER 500 Study. *J. Clin. Oncol.* **2024**, *42*, 3692–3701. [CrossRef] [PubMed]

[109] Walker, C.; Angelo, M. Toward Clinical Applications of Spatial-Omics in Cancer Research. *Nat. Cancer* **2024**, *5*, 1771–1773. [CrossRef] [PubMed]

[110] FDA-NIH Biomarker Working Group. Validation. In: *BEST (Biomarkers, EndpointS, and other Tools) Resource* [Internet]. Silver Spring, MD: Food and Drug Administration (US); 2017 – Co-published by National Institutes of Health (US), Bethesda, MD. Updated 16 November 2020. Available online: https://www.ncbi.nlm.nih.gov/books/NBK464453/ (accessed on 13 September 2026).

[111] Albert, N.L.; Galldiks, N.; Ellingson, B.M.; van den Bent, M.J.; Chang, S.M.; Cicone, F.; Koh, E.-S.; Law, I.; Le Rhun, E.; Mair, M.J.; et al. RANO Criteria for Response Assessment of Brain Metastases Based on Amino Acid PET Imaging. *Nat. Med.* **2025**, *31*, 1424–1430. [CrossRef] [PubMed]

[112] Verger, A.; Tolboom, N.; Cicone, F.; Chang, S.M.; Furtner, J.; Galldiks, N.; Gempt, J.; Guedj, E.; Huang, R.Y.; Johnson, D.R.; et al. Joint EANM/EANO/RANO/SNMMI Practice Guideline/Procedure Standard for PET Imaging of Brain Metastases: Version 1.0. *Eur. J. Nucl. Med. Mol. Imaging* **2025**, *52*, 1822–1839. [CrossRef] [PubMed]

[113] Galldiks, N.; Abdulla, D.S.Y.; Scheffler, M.; Wolpert, F.; Werner, J.M.; Hüllner, M.; Stoffels, G.; Schweinsberg, V.; Schlaak, M.; Kreuzberg, N.; et al. Treatment Monitoring of Immunotherapy and Targeted Therapy Using ^{18}F-FET PET in Patients with Melanoma and Lung Cancer Brain Metastases: Initial Experiences. *J. Nucl. Med.* **2021**, *62*, 464–470. [CrossRef] [PubMed]

[114] Kotecha, R.; Chiang, V.; Tom, M.C.; Parent, E.; Nabavizadeh, A.; Siegel, B.A.; Huang, J.; Zan, E.; Peddi, S.; Brem, S.; et al. ^{18}F-Fluciclovine for Detection of Recurrent Brain Metastases After Radiation Therapy: Image Interpretation Criteria and Diagnostic Performance From the PURSUE Study. *Int. J. Radiat. Oncol. Biol. Phys.* **2026**, *125*, 1410–1420. [CrossRef] [PubMed]

[115] Ciavarra, B.; Krayyem, A.; Ansari, S.; Shindell, E.; Gule-Monroe, M.K.; Patel, C.B.; Johnson, J.M. Delayed ^{18}F-FDG PET for the Evaluation of Suspected Recurrent Disease in Brain Metastases Treated with Radiation. *Clin. Radiol.* **2026**, *99*, 107390. [CrossRef] [PubMed]

[116] Li, M.; Chen, J.; Zhang, B.; Yu, J.; Wang, N.; Li, D.; Shao, Y.; Zhu, D.; Liang, C.; Ma, Y.; et al. Dynamic Monitoring of Cerebrospinal Fluid Circulating Tumor DNA to Identify Unique Genetic Profiles of Brain Metastatic Tumors and Better Predict Intracranial Tumor Responses in Non-Small Cell Lung Cancer Patients with Brain Metastases: A Prospective Cohort Study (GASTO 1028). *BMC Med.* **2022**, *20*, 398. [CrossRef] [PubMed]

[117] Lee, J.H.; Menzies, A.M.; Carlino, M.S.; McEvoy, A.C.; Sandhu, S.; Weppler, A.M.; Diefenbach, R.J.; Dawson, S.-J.; Kefford, R.F.; Millward, M.J.; et al. Longitudinal Monitoring of ctDNA in Patients with Melanoma and Brain Metastases Treated with Immune Checkpoint Inhibitors. *Clin. Cancer Res.* **2020**, *26*, 4064–4071. [CrossRef] [PubMed]

[118] Voglis, S.; Schulz, D.; Eling, N.; De Souza, N.; Regli, L.; Neidert, M.C.; Czabanka, M.; Weller, M.; Le Rhun, E.; Mihic-Probst, D.; et al. Spatially-Resolved Single-Cell Imaging of Melanoma Brain Metastases Identifies Localized Immune Patterns Predictive of Immune Checkpoint Blockade Response. *Neuro Oncol.* **2026**, *28*, 2211–2223. [CrossRef] [PubMed]

[119] Zhu, J.; Ye, J.; Ma, Y.; Lin, Z.; Wen, Y.; Sheng, J.; Yang, M. Spatial Immune Atlas of Breast Cancer Brain Metastasis Reveals CD163+ Macrophage Reprogramming Associated with Immune Escape. *J. Immunother. Cancer* **2026**, *14*, e014421. [CrossRef] [PubMed]

[120] Khatri, A.; McKernan, C.M.; Van Swearingen, A.E.D.; Jain, V.; Thrash, H.L.; Towne, A.; Gu, J.J.; Gregory, S.G.; Anders, C.K.; Pendergast, A.M. Spatially Resolved Transcriptomics in Human Brain Metastases Identifies Macrophage-Tumor Interactions Associated with Survival. *iScience* **2026**, *29*, 116517. [CrossRef] [PubMed]

[121] Cheng, X.; Patel, K.K.; Zhou, B.; Fu, Y.; Cleary, R.T.; Highkin, M.; Hsia, J.; Jin, X.; Kohn, B.; Prior, J.L.; et al. Interleukin-34–Induced Arg1+ Macrophages Play a Key Role in Breast Cancer Brain Metastasis. *Cancer Res. Commun.* **2026**, *6*, 1388–1404. [CrossRef] [PubMed]

[122] Sadik, A.; Somarribas Patterson, L.F.; Öztürk, S.; Mohapatra, S.R.; Panitz, V.; Secker, P.F.; Pfänder, P.; Loth, S.; Salem, H.; Prentzell, M.T.; et al. IL4I1 Is a Metabolic Immune Checkpoint That Activates the AHR and Promotes Tumor Progression. *Cell* **2020**, *182*, 1252–1270.e34. [CrossRef] [PubMed]

[123] Ahn, J.Y.; Dong, W.; Puri, A.; Vasquez, M.; Raghunathan, R.; Yang, L.; Sheng, J.; Zhao, H.; Wong, S.T.C. Spatial Cross-talk Modeling of the Tumor Microenvironment Identifies CCR5-Mediated Glia-to-Glia Signaling as a Key Regulator of Brain Metastatic Progression. *Cancer Res.* **2025**, *85*, 4839–4855. [CrossRef] [PubMed]

[124] Su, R.; Ma, X.; Guo, X.; Huang, S.; Liu, R.; Song, Z.; Gao, H.; Zhao, K.; Li, Y.; Liang, K. Impact of Cold Ischemia on the Proteome and Metabolome of Tissue Samples and Preanalytical Quality Control Using Mass Spectrometry Imaging. *J. Proteome Res.* **2025**, *24*, 2968–2980. [CrossRef] [PubMed]

[125] Brastianos, P.K.; Carter, S.L.; Santagata, S.; Cahill, D.P.; Taylor-Weiner, A.; Jones, R.T.; Van Allen, E.M.; Lawrence, M.S.; Horowitz, P.M.; Cibulskis, K.; et al. Genomic Characterization of Brain Metastases Reveals Branched Evolution and Potential Therapeutic Targets. *Cancer Discov.* **2015**, *5*, 1164–1177. [CrossRef] [PubMed]

[126] Valiente, M.; Aydoğan, L.E.; Feigin, N.; Gahn, C.; Hernandez-Oliver, C.; Milling, F.; Oktem, E.; Ortega-Sabater, C.; Priego, N.; Ricci, A.A.; et al. Patient-Derived Resources for Decoding and Targeting Brain Metastases Ecosystems. *EMBO Mol. Med.* **2026**, *18*, 3017–3027. [CrossRef] [PubMed]

[127] Gan, S.; Macalinao, D.G.; Shahoei, S.H.; Tian, L.; Jin, X.; Basnet, H.; Bibby, C.; Muller, J.T.; Atri, P.; Seffar, E.; et al. Distinct Tumor Architectures and Microenvironments for the Initiation of Breast Cancer Metastasis in the Brain. *Cancer Cell* **2024**, *42*, 1693–1712.e24. [CrossRef] [PubMed]

[128] Greenwald, N.F.; Nederlof, I.; Sowers, C.; Ding, D.Y.; Park, S.; Kong, A.; Houlahan, K.E.; Varra, S.R.; de Graaf, M.; Geurts, V.; et al. Temporal and Spatial Composition of the Tumor Microenvironment Predicts Response to Immune Checkpoint Inhibition in Metastatic TNBC. *Nat. Cancer* **2026**, *7*, 435–450. [CrossRef] [PubMed]

[129] Li, M.; Wang, T.; Zhang, Z.; Dongye, Y. Metabolic Reprogramming in the Post-Metastatic Tumor Microenvironment: Multi-Omics Insights Into Determinants of Immunotherapy Response. *Front. Immunol.* **2026**, *16*, 1742855. [CrossRef] [PubMed]

[130] Zemaitis, K.J.; Paša-Tolić, L. Challenges in Spatial Metabolomics and Proteomics for Functional Tissue Unit and Single-Cell Resolution. *Semin. Nephrol.* **2024**, *44*, 151583. [CrossRef] [PubMed]

[131] Haque, S.Y.; Shatabda, S.; Islam, S.; Dipu, S.A.; Azim, R. The Good, the Bad, and the Ugly: Opportunities, Challenges, and Pitfalls in Spatial Proteomics Modeling. *Brief. Bioinform.* **2026**, *27*, bbag169. [CrossRef] [PubMed]

[132] Saunders, K.D.G.; Lewis, H.-M.; Beste, D.J.V.; Cexus, O.; Bailey, M.J. Spatial Single Cell Metabolomics: Current Challenges and Future Developments. *Curr. Opin. Chem. Biol.* **2023**, *75*, 102327. [CrossRef] [PubMed]

[133] Luo, M.; Kou, T.; Yin, Y.; Zhou, S.; Zhu, X.; Zeng, X.; Hu, J.; Zhu, Z.-J. Deep-Coverage Single-Cell Metabolomics Enabled by Ion Mobility-Resolved Mass Cytometry. *Nat. Methods* **2026**, *23*, 585–595. [CrossRef] [PubMed]

[134] Jang, C.; Chen, L.; Rabinowitz, J.D. Metabolomics and Isotope Tracing. *Cell* **2018**, *173*, 822–837. [CrossRef] [PubMed]

[135] Schwaiger-Haber, M.; Stancliffe, E.; Anbukumar, D.S.; Sells, B.; Yi, J.; Cho, K.; Adkins-Travis, K.; Chheda, M.G.; Shriver, L.P.; Patti, G.J. Using Mass Spectrometry Imaging to Map Fluxes Quantitatively in the Tumor Ecosystem. *Nat. Commun.* **2023**, *14*, 2876. [CrossRef] [PubMed]

[136] Fan, T.W.; Lane, A.N.; Higashi, R.M. Stable Isotope Resolved Metabolomics Studies in ex vivo Tissue Slices. *Bio-Protocol* **2016**, *6*, e1730. [CrossRef] [PubMed]

[137] Zhou, Y.; Xiao, X.; Dong, L.; Tang, C.; Xiao, G.; Xu, L. Cooperative Integration of Spatially Resolved Multi-Omics Data with COSMOS. *Nat. Commun.* **2025**, *16*, 27. [CrossRef] [PubMed]

[138] Liu, Y.; Wang, C.; Wang, Z.; Chen, L.; Li, Z.; Song, J.; Zou, Q.; Gao, R.; Qian, B.-Z.; Feng, X.; et al. High-Parameter Spatial Multi-Omics Through Histology-Anchored Integration. *Nat. Methods* **2026**, *23*, 373–386. [CrossRef] [PubMed]

[139] Roy, S.; Nassor, M.; Zahin, F.; Chaudhry, S.; Odei, K.P.K.; Nkrumah-Boateng, P.A.; Wireko, A.A. Leveraging Single-Cell and Spatial Omics for Brain Tumour Insights to Improve Therapeutic Strategies. *Mol. Brain* **2026**, *19*, 61. [CrossRef] [PubMed]

Disclaimer/Publisher's Note: The views expressed in this article are those of the author(s) and do not necessarily reflect the views of the publisher or editors. The publisher and editors assume no responsibility for any injury or damage resulting from the use of information contained herein.